Cellulose Nanocrystal Coated Paraffin Wax Coating for Fog and Dew Water Harvesting

by

Riyao Yan

A thesis
presented to the University Of Waterloo
in fulfilment of the
thesis requirement for the degree of
Master of Applied Science
in
Chemical Engineering

Waterloo, Ontario, Canada, 2026

© Riyao Yan 2026

Author's Declaration

I hereby declare that I am the sole author of this thesis. This is a true copy of the thesis, including any required final revisions, as accepted by my examiners. I understand that my thesis may be made electronically available to the public.

Abstract

Fresh water scarcity is an urgent global issue. A sustainable and renewable method is harvesting atmospheric water, among which fog and dew water can be passively collected onto a surface. The efficiency of such collecting systems depends critically on the wetting and dynamic behavior of water droplets on the surface. Common approaches to modify surface topography and hydrophobicity often relies on lithographic, plasma, or fluoropolymer-based methods that are costly, complex, and environmentally unsustainable. In contrast, this work proposes a novel, simple, and bottom-up approach for producing surface with functional coatings through cellulose nanocrystal (CNC)–stabilized Pickering emulsions.

The first part of the study focuses on understanding the stabilization and formulation behavior of CNC-based oil-in-water emulsions under varying CNC concentration, ionic strength, and oil-to-water ratios. The resulting interfacial coverage and droplet packing efficiency govern the size and assembly of the wax microparticles, allowing fine control of surface roughness and wettability. Coatings derived from these particles exhibit a wide range of wetting states—from hydrophilic to superhydrophobic—depending on CNC surface coverage and aggregation state.

In the second part, these coatings are evaluated for fog and dew water collection, emphasizing the differences between liquid water deposition and humid air condensation on surface. The results show that overall water collection performance is governed by two coupled processes: the rate at which moisture is captured on the surface and the efficiency with which the accumulated water is removed. Previous studies have shown that while superhydrophobic surfaces exhibit superior droplet removal efficiency, their performance can degrade under continuous usage due to partial loss of superhydrophobicity and water film formation. On the other hand, surfaces with balanced nucleation density and drainage efficiency are more desirable, especially for condensation.

This research establishes a biobased, PFAS-free, and scalable fabrication route for tailoring surface wettability using CNC-stabilized emulsions. Beyond atmospheric water harvesting, the insights gained here into interfacial assembly and condensation dynamics under realistic humid-air conditions contribute broadly to the design of sustainable coatings for humidity control and anti-fogging/anti-icing applications.

Acknowledgements

AI tool (GPT-5 and GPT-5.1, OpenAI, accessed October–November 2025) was used during the drafting process to support grammar refinement and structural feedback. All analysis, interpretation, and original writing were completed by the author.

Table of Contents

Author's Declaration ..... *ii*
Abstract ..... *iii*
Acknowledgements ..... *iv*
List of Figures ..... *viii*
List of Tables ..... *x*
List of Abbreviations ..... *xi*
Chapter 1 Introduction *1*
1.1 Overview **1**
1.2 Objectives **1**
1.3 Outline of thesis **2**
Chapter 2 Literature Review: Engineered Surfaces for Atmospheric Water Harvesting *3*
2.1 Background and motivation **3**
2.1.1 Atmospheric water as a sustainable resource 3
2.1.2 AWH technologies overview 3
2.2 Fog and dew harvesting **5**
2.2.1 Formation mechanism and conventional collecting devices 5
2.2.2 Limiting factors for water harvesting performance 6
2.2.3 Inspiration of performance enhancement from nature 7
2.3 Enhancing AWH via engineering surface wettability & topography **9**
2.3.1 Wetting as a contact angle phenomenon 9
2.3.2 Droplet dynamics on surface 12
2.3.3 Surface with patterned wetting properties 14
2.3.4 Surface with micro-nano structures 16
2.4 Condensation mode and practical AWH design **17**
2.4.1 DWC is the target for surface designs 17
2.4.2 The lack of comprehensive comparison for humid air condensation 18
2.4.3 Role of non-condensable gases in condensation 19
2.5 Summary and implication for current project **21**
Chapter 3 CNC-coated Wax Microparticles: Variation in Synthesis Formula *23*
3.1 Introduction **23**

3.2 Experimental **24**
3.2.1 Raw materials 24
3.2.2 Emulsion synthesis procedure 24
3.2.3 Emulsion characterization 26
3.3 CNC and NaCl formulation **26**
3.3.1 Ionic strength and CNC aggregation in aqueous dispersion 26
3.3.2 CNC concentration in aqueous dispersion 30
3.3.3 Oil phase fraction 33
3.4 CNC and ODA formulation **35**
3.4.1 Electrostatic and hydrophobic adsorption of ODA on CNC 36
3.4.2 ODA concentration in emulsion 37
3.5 Conclusions **41**
Chapter 4 Wax Microparticle Coatings: Performance Comparison between Fog and Dew Water Harvesting ***42***
4.1 Introduction **42**
4.2 Experimental **43**
4.2.1 Surface fabrication procedure 43
4.2.2 Surface characterization 43
4.2.3 Fog water harvesting tests 44
4.2.4 Humid air condensation test 44
4.3 Static and dynamic contact angle **45**
4.3.1 Static contact angle 45
4.3.2 Contact angle hysteresis 47
4.3.3 Selection of coating for water harvesting 48
4.4 Fog water harvesting results **49**
4.5 Condensation results **51**
4.6 Conclusions **52**
Chapter 5 Conclusions ***54***
5.1 Conclusions **54**
5.2 Future work **55**
5.2.1. Remaining questions in Pickering emulsion design 55
5.2.2. Remaining questions in water harvesting mechanisms 55

5.2.3. Integration, durability, and applications 56
References ***57***
Appendix: Error Analysis of CNC-wax Pickering Emulsion Particle Size Measurement ***61***
Objective of error analysis 61
Sources of uncertainty 61
Quantification of Particle Size Distribution Width 62

List of Figures

Figure 1. Overview of atmospheric water harvesting technologies, their classifications, and schematics of fundamental process. 4
Figure 2. Biomimetic inspirations: water collection mechanism of desert beetle, cactus, and moss awn 7
Figure 3. Schematic drawings for solid surface wetting phenomenon and their correlation with the limiting factors in water harvesting performance 9
Figure 4. Schematic drawings of droplet nucleation, growth, and departure on vertically placed surface (side view) to illustrate dropwise and filmwise water drainage approach for fog and dew water harvesting. 12
Figure 5. Surfaces with special design in wetting properties that enhance water harvesting performance 15
Figure 6. Surfaces with micro-nano structures 16
Figure 7. Schematics of condensation modes. 17
Figure 8. heat transfer models of vapor condensation in presence of NCGs for analysis of individual contribution of temperature drop: 19
Figure 9. Schematic drawing of oil in water emulsion particle stabilized by surfactants vs. Pickering emulsion particle stabilized by solid particles 24
Figure 10. Synthesis procedure of CNC-coated solid wax microparticle suspended in water 25
Figure 11. 1 wt% CNC dispersed in different NaCl solution (left to right: 0, 9, 17, 43, 85, 170 mM NaCl): a) picture of dispersion; b) zeta potential measurements. 27
Figure 12. CNC-coated wax microparticle suspensions 28
Figure 13. Optical microscopy images of CNC-coated wax microparticles (salt formulation, varying CNC and NaCl concentration) 29
Figure 14. CNC-coated wax microparticle suspensions 31
Figure 15. SEM images of CNC-coated wax microparticles (salt formulation) 32
Figure 16. peak particle size measurements of CNC-coated wax microparticle suspensions. synthesis formula: a) 1 and 1.5 wt% CNC in 43 mM NaCl solutions, varying oil fraction; b) constant CNC to oil mass ratio, 43 mM NaCl solutions, varying oil fraction. 33

Figure 17. Optical microscopy images of CNC-coated wax microparticles (salt formulation, varying CNC concentration and oil fraction)..... 35
Figure 18. electrostatic interaction between sulfate ester group on CNC and protonated amine group of ODA..... 36
Figure 19. zeta potential measurements of 1 wt% CNC dispersed in different ODA solution of pH =3 (left to right: 0, 0.05, 0.1, 0.25, and 0.5 wt% ODA) 36
Figure 20. peak particle size measurements of CNC-coated wax microparticle suspensions (10% oil fractions, varying ODA/oil and ODA/CNC ratio) 37
Figure 21. Optical microscopy images of CNC-coated wax microparticles (surfactant formulation) 39
Figure 22. SEM images of CNC-coated wax microparticles (surfactant formulation)..... 40
Figure 23. Spray coating procedure 43
Figure 24. fog harvesting test set up..... 44
Figure 25. condensation test set up 45
Figure 26. average static contact angle measurements of coated surfaces. Synthesis formulation: a) 43 mM NaCl, 10% oil fraction, varying CNC; b) 10% oil fraction, varying ODA and CNC. 46
Figure 27. Static contact angle vs. contact angle hysteresis of coated surfaces. Synthesis formulation: 10% oil fraction, varying ODA and CNC. 49
Figure 28. collected water vs. fog exposure time..... 51
Figure 29. collected water vs. surface cooling time..... 52
Figure A. Particle size distribution. Emulsion formula: 0.5% CNC, 47 mM NaCl, 15% oil fraction. a) single measurement of multiple emulsion samples; b) multiple measurements of one emulsion sample..... 62

List of Tables

Table 1. CNC-coated wax Pickering emulsion formula 25
Table A. Characteristic particle size metrics extracted from particle size distributions 62

List of Abbreviations

abbreviation	definition
AWH	atmospheric water harvesting
CA	static contact angle
CAH	contact angle hysteresis
CNC	cellulose nanocrystal
DWC	dropwise condensation
HCl	hydrochloric acid
HTC	heat transfer coefficient
NaCl	sodium chloride
NCG	non-condensable gas
o/w	oil in water
ODA	octadecylamine
OH	hydroxyl group
RH	relative humidity
SEM	scanning electron microscope
SHB	superhydrophobic
SHL	superhydrophilic
TPCL	three phase contact line

Chapter 1 Introduction

1.1 Overview

There has been an increasing need for sustainable and decentralized clean water generation technologies due to the urgent global water scarcity issue. Atmospheric water is a ubiquitous and abundant source, and its collection does not require large-scale, energy-intensive infrastructures. Therefore, atmospheric water harvesting (AWH), with fog and dew water being the common source, presents itself as a passive and renewable strategy that can supplement fresh water without geographical restrictions. In this thesis, dew water refers specifically to liquid water formed by condensation of atmospheric vapor on a surface cooled below the dew point, rather than suspended microdroplets in air.

To develop efficient AWH devices, the most critical role is building a surface that can capture moisture from fog/humid air and drain the collected liquid water. Current research is mostly inspired by plants and animals, such as lotus leaf and desert beetle, and they mimic the natural water collecting mechanisms. The growing emphasis in functional coatings and green fabrication methods reflects the evolving role of material science in bridging fundamental understanding of interfacial phenomena with practical solutions in sustainability.

Developing efficient water harvesting surfaces commonly relies on complex lithographic or fluorinated fabrication methods that are costly, non-scalable, or environmentally harmful. Bio-based materials, such as cellulose nanocrystal (CNC), offer exciting research opportunities for creating tunable, textured, biphilic coatings. Even though CNC has been studied for stabilizing Pickering emulsions, there remain limited understanding of how CNC can be systematically tailored to achieve the desired emulsion particle properties and surface morphology for AWH devices. Another major knowledge gap is the analysis of fog vs. dew water harvesting behavior and their impact on surface hydrophobicity change during operation. This study aims to contribute to the understanding of these two aspects by establishing correlation between formulation, surface structure, and water collection performance.

1.2 Objectives

This thesis focuses on both material development and performance evaluation, aiming to investigate coatings synthesized from CNC-wax oil-in-water (o/w) Pickering emulsion of varying

formulations and testing their application in collecting fog and dew water. The specific objectives are:

1.2.1 Prepare CNC-stabilized o/w Pickering emulsions by systematically varying CNC concentration, salt concentration, oil-to-water ratio, and surfactant concentration. Examine how formulation parameters influence emulsion stability, droplet size distribution, and interfacial coverage.

1.2.2 Fabricate coatings from the emulsions via spray coating method. Characterize surface morphology, roughness, and wettability using contact angle measurements.

1.2.3 Observe the droplet dynamics on coated surface under controlled dew condensation and fog flow conditions. Establish structure, property, performance relationships linking formulation parameters, surface features, and water collection efficiency.

1.3 Outline of thesis

This thesis consists of the following chapters: Chapter 1 introduces the background and motivation for this project. Chapter 2 conducts a literature review on surface engineering technologies for fog and dew water harvesting. Chapter 3 studies the Pickering emulsion formulation. Chapter 4 evaluates the coating performance. Chapter 5 concludes the key findings and suggests future research directions.

Chapter 2 Literature Review: Engineered Surfaces for Atmospheric Water Harvesting

2.1 Background and motivation

2.1.1 Atmospheric water as a sustainable resource

Fresh water scarcity is an urgent global issue. Over 2 billion people worldwide lack access to safely managed drinking water. Freshwater resources are unevenly distributed, with many arid and semi-arid regions facing chronic shortages. [1], [2], [3] Current large-scale solutions, such as desalination, are energy-intensive, costly, and environmentally impactful. Decentralized systems can reduce dependence on large-scale infrastructure, which is especially favorable for rural and remote areas. In addition, UN SDG 6: Clean Water and Sanitation calls for innovative, low-carbon water technologies. [4] A sustainable and renewable solution is harvesting water from the atmosphere, as atmospheric water is ubiquitously available, even in arid regions. Atmospheric water harvesting (AWH) technologies are suitable for point-of-use system and are compatible with passive operation, such as radiative cooling, or hybrid active/passive designs. [2]

2.1.2 AWH technologies overview

AWH technologies can be divided into these general types: 1) harvesting water from cloud, rain, and fog; 2) capturing and condensing vapor from humid air via direct dewing; 3) membrane separation; and 4) sorbent sorption.

Rain and fog water are among the most widely explored passive AWH methods. Both are low cost and energy independent, but their efficiency is strongly dependent on local meteorological conditions, such as wind speed, fog density, relative humidity, nighttime cooling efficiency, etc. [5] Cloud seeding is the artificial enhancement of precipitation from clouds by dispersing substances such as silver iodide into the atmosphere. These particles act as nuclei for condensation of ice crystals and promote rainfall under suitable cloud conditions. The concerns with this method are its high cost, unpredictable efficiency, and potential environmental impact. [2]

Direct dewing involves cooling the surface below the dew point temperature and allowing the water in humid air to condense directly on the surface. The cooling can be achieved either passively through radiative or evaporative cooling, or active via refrigeration. [6], [7]

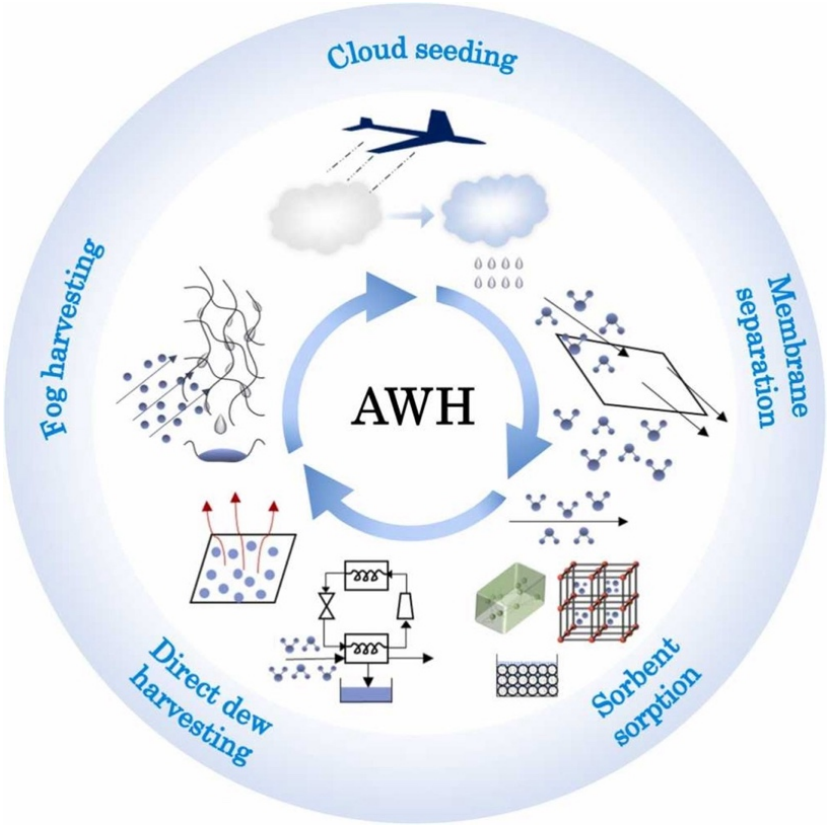


Figure 1. Overview of atmospheric water harvesting technologies, their classifications, and schematics of fundamental process. Reproduced from [2].

Membrane separation operates by selectively allow water vapor to permeate through the membrane while rejecting other gases. It can also be combined with passive or active cooling systems to condense the permeated vapor. The challenges with this novel method remain in terms of durability and scalability. [2]

Sorbent sorption methods use hygroscopic or porous adsorption materials, which are functionalized with hydroxyl or other polar groups to attract water droplets. Subsequently, the desorption process is driven by thermal or solar energy, releasing concentrated water vapor that can be condensed and collected. However, such systems often require additional energy input for regeneration cycles. [2], [8], [9]

Depending on the availability of the water in the atmosphere and the amount of energy input in running the AWH system, the amount of water collected varies greatly. There has been

continuous effort in the development of AWH systems that are made from sustainable materials, use only renewable energy, and with good performance under various environmental conditions.

2.2 Fog and dew harvesting

2.2.1 Formation mechanism and conventional collecting devices

Fog & mesh collectors

Fog is a weather phenomenon that occurs when water vapor in the air condenses into tiny liquid droplets that remain suspended near the ground. During nighttime, Earth's surface radiates heat into space, causing the ground temperature to be cooled. Fog forms when the air close to the ground is saturated with moisture and cooled to the dew point. Water vapor in the cooled air condenses into microdroplets with typical diameter of 1 to 40 μm. These condensed microdroplets remain suspended in the air, and they can be captured using fog collectors. The collectors are vertical mesh nets, usually made of materials such as polypropylene. Fog mesh is a passive AWH method with low maintenance requirements. However, harvesting fog water can only work in specific places where fog is regular and predictable, such as in coastal regions, mountains, and deserts. As a result, this method is less accessible than seawater on a large scale. [5] The water yield also depends on fog density, wind speed, and mesh design. A 1 cubic meter of foggy air can contain between 0.05 and 0.5 grams of water.

Dew & radiative condensers

Dew water can be harvested and used similarly to fog water in places with high humidity and clear skies. However, compared with capturing fog, which is collecting condensed water droplets in the air, the capture of dew water has a different physical process. When the surface cools below the dew point, water vapor in the air can directly condenses onto surface as liquid water. Dew is the moisture that condenses into water droplets on cool surface, such as grass, leaves, or metal, usually overnight. Dew collection is a more promising strategy than fog harvesting for the water scarcity problem, specifically in arid regions, despite its lower output. [10]

The additional phase change from vapor to liquid requires different capture method and condition for dew water. Radiative condenser is a passive method to collect dew. The ideal conditions for dew formation requires high relative humidity at night and surface that cool fast. Therefore, the surface of condensers is made of materials that radiate heat well and cool below the dew point for water condensation. [11]

2.2.2 Limiting factors for water harvesting performance

As fog and dew water harvesting are both extracting the moisture in the humid air into liquid water, the collecting devices have similar designs in surface properties to obtain optimal water collection performance. However, there are also differences due to the intrinsic formation mechanism difference of fog and dew. Fog has higher quantity of available water, and the design should focus on the fast removal of water on the surface. The main limitation of improving a fog mesh's efficiency is the droplet mobility on the surface, which can be measured as the droplet shedding rate. A common approach to improve the configuration usually involves the use of hydrophobic coatings to reduce droplet pinning to the surface and facilitate faster water drainage. [12]

On the other hand, dew is fundamentally different than fog in that it has lower availability of water and the phase change of vapor to liquid on the surface of the collecting device.[6] Dew harvesting is limited by the low water flux intake. In addition, the rate of heat loss from the surface constrains passive cooling performance. The process of atmospheric moisture extraction via formation of dew on a surface can be impacted by various environmental conditions. When the dew point is much lower than ambient air temperature, most of the radiative cooling is consumed by a sensible heat exchange, causing very low dew yield.[5] Therefore, existing passive dew condensers can only be a supplementary water source in regions with favorable conditions. Energy efficient dew harvesting requires the condenser surface to be able to both capture and remove water. It requires a different surface design with both hydrophilic and hydrophobic properties to improve water nucleation and removal rates.

Active cooling and moisture harvesting index (MHI)

For AWH via condensation, instead of using passive cooling such as the radiative condenser, electric compression expansion or thermoelectric systems can be used to further cool the surface below dew point and promote the formation of liquid water. Active systems can produce a more reliable quantity of water under a wide range of environmental conditions. However, the challenges are that it is energy-intensive and costly.

The moisture harvesting index (MHI) is defined as the ratio of the energy invested in the desired water condensation process to the total energy invested in the cooling of the condensable and non-condensable gases in the air bulk. There is considerable variation in MHI due to meteorological conditions.[5]

2.2.3 Inspiration of performance enhancement from nature

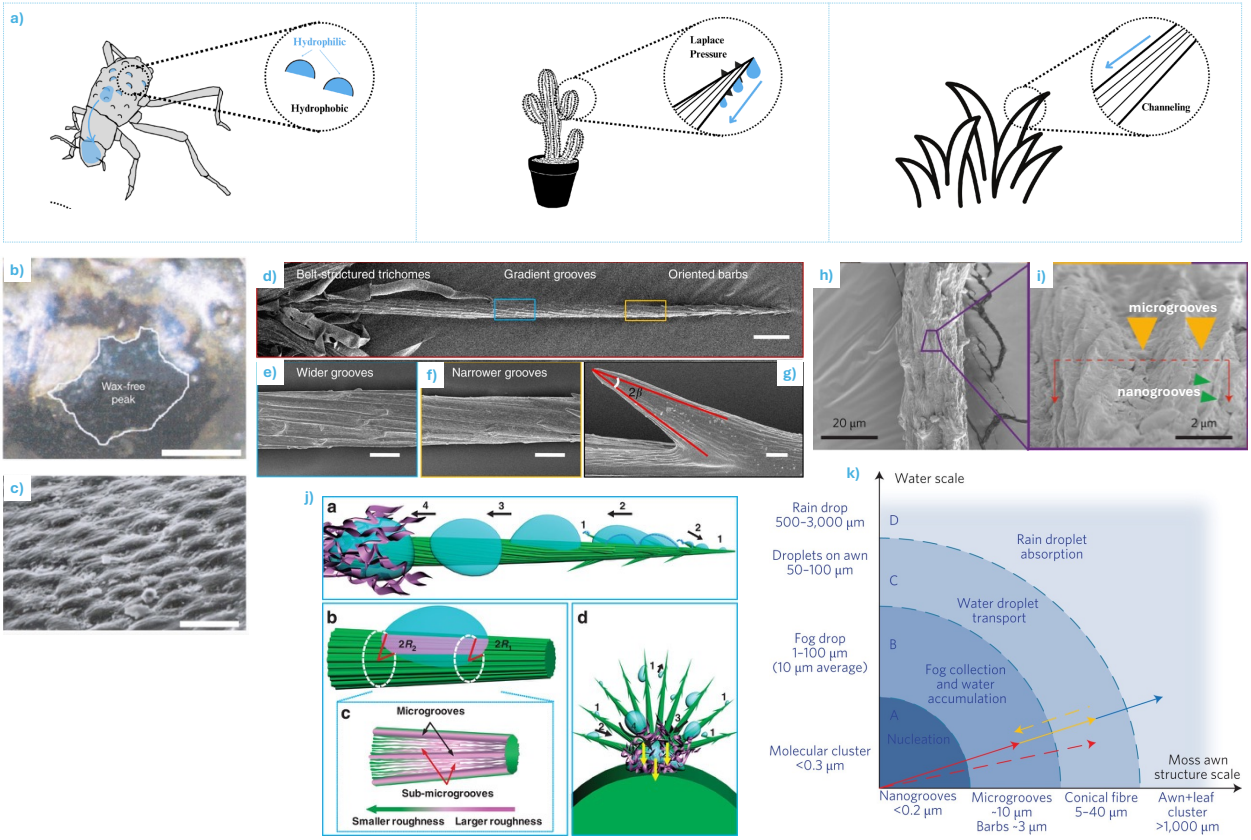


Figure 2. Biomimetic inspirations: a) schematic of water collection mechanism of desert beetle, cactus, and moss awn (adapted from [13]); b) wax testing procedure showing the peaks of the "bump" on the elytra are wax-free (scale bar = 0.2 mm); c) SEM of the textured surface (scale bar = 10 □m) (adapted from [14]); d), e), f) & g) SEM of cactus spine. g) magnified image of a single barb (scale bars = 100 μm (d), 20 μm (e–f) and 2 μm (g). ; j) water collection and transport mechanism of cactus: droplets preferentially condense at the spine tip, where Laplace pressure gradients and surface energy gradients drive directional motion toward the base (adapted from [15]); h) & i) tilted high-magnification photograph of SEM of the surface of the moss awn showing micro- and nanogrooves structures (adapted from [16]); k) multifunctional hierarchical water harvest mechanisms: the concentric shaded areas illustrate the size scales of the moss awn structures vs. the size scale of the water that each functional structures collect; the arrows show these hierarchical mechanisms work together to capture water available at different scales (adapted from [16]).

Desert beetle & fog capture

One of the most widely studied biomimetic inspirations for designing AWH systems is the desert beetle. It is famous for its ability to survive in the Namib Desert where rainfall is negligible, but morning fog is a frequent and reliable source of atmospheric moisture. The strategy of the beetle relies on the unique hybrid wettability of its dorsal elytra, which consist of smooth, wax-free

hydrophilic peaks surrounded by wax-coated hydrophobic troughs. Microscopic fog droplets preferentially nucleate and grow on the hydrophilic peaks, while the surrounding hydrophobic background prevents excessive spreading and facilitates droplet mobility. Once droplets reach a critical size (~4–5 mm in diameter), gravitational and aerodynamic forces overcome surface adhesion, causing them to roll down the beetle's tilted body toward its mouthparts. [14]

Inspired by the beetle surface's ability to balance water droplet capture and drainage, various artificial surfaces that mimic its alternating hydrophilic and hydrophobic patterning have been fabricated and studied. With hydrophilic patches to promote droplet nucleation and hydrophobic regions to facilitate water transport, these designs can collect more fog water compared with surfaces of uniform wettability. This indicates a promising route toward passive, material-driven devices of high fog harvesting efficiency. [13], [17]

Multifunctional system of desert moss and cactus & extraction of water from humid air

Desert plants also possess highly evolved water conservation and transport systems. The cactus *Opuntia microdasys* employs a multi-structural and multi-functional system for efficient fog capture. Its spines consist of oriented barbs at the tip, gradient grooves along the shaft, and belt-structured trichomes at the base. These features act in sequence to deposit, collect, transport, and absorb water. The conical shape of the spines and their grooves establish a Laplace pressure gradient and a surface-free energy gradient that drive droplets directionally from the tip toward the base. [15]

Laplace pressure refers to the curvature-induced pressure difference across a droplet's liquid–vapor interface, and on rough or nanostructured surfaces it plays a central role in how small condensate droplets deform, migrate, and eventually detach. It is given by:

$$\Delta P = \gamma\left(\frac{1}{R_1} + \frac{1}{R_2}\right)$$

Droplets confined within re-entrant or asymmetric textures develop curvature gradients between constrained and unconstrained regions of the droplet. During growth, these curvature differences generate internal Laplace-pressure gradients that act as directional capillary forces, enabling droplets to depin, reorient, or climb through complex microcavities. [15], [18], [19] This makes Laplace-pressure-driven capillarity a key mechanism underlying robust droplet removal and sustained dropwise condensation on rough, multiscale surfaces.

Another notable plant is the desert moss *Syntrichia caninervis,* which thrives in extremely arid regions despite lacking true roots or vascular tissue. Unlike other plants that primarily rely on fog harvesting, the moss has a unique adaptation of its leaf structure to collect water from multiple

sources and promote nucleation from humid air. The tiny hair (awn) on the end of the leaf is a multiscale structure equipped for four coupled modes of water collection and transport Nucleation is considered the smallest scale of water capture, which involves the heterogeneous nucleation of liquid dew droplet from a saturated gas phase. The longitudinal nanogrooves on the awn reduce the nucleation barrier, allowing dew droplets to condense efficiently when the air reaches saturation. At the microscale, grooves and clusters of barbs trap and coalesce fog droplets into larger drops, while the conical geometry of the awn drives directional transport of water toward the leaf base. Rainfall is the largest scale of water source. The high density of awn clusters can retain falling droplets by reducing the losses from splashing. [16] Such unique multiscale structure of the desert moss illustrates a strategy of broad-spectrum moisture collection system that integrate dew nucleation with fog capture. This is particularly relevant for engineered surface aimed at harvesting water from diverse atmospheric sources.

2.3 Enhancing AWH via engineering surface wettability & topography

2.3.1 Wetting as a contact angle phenomenon

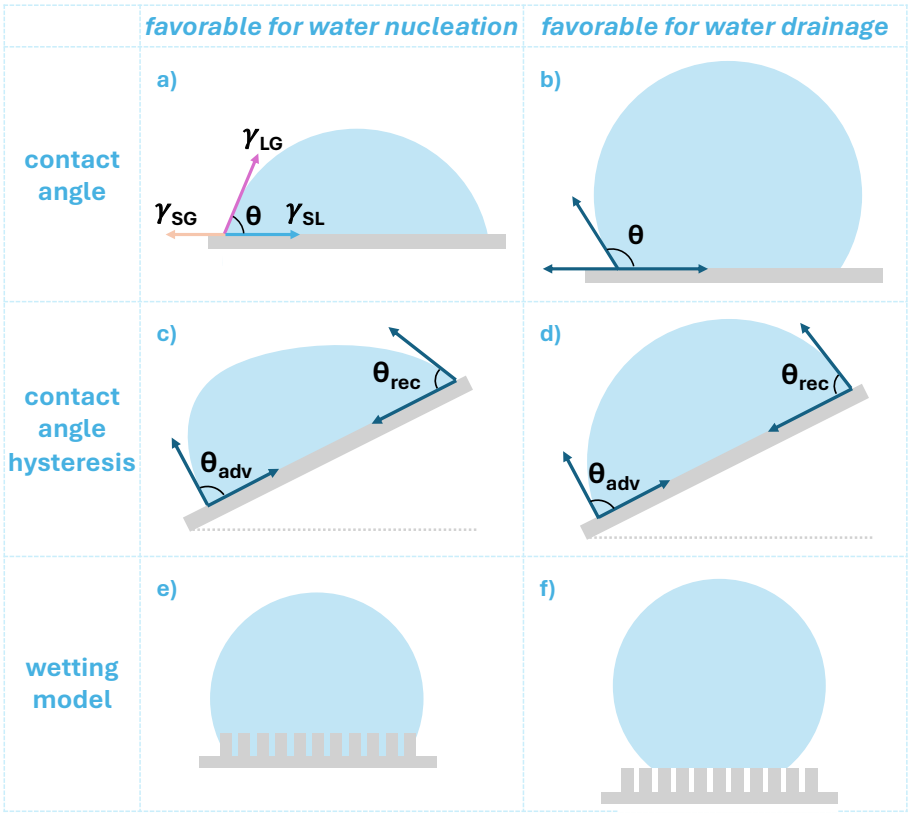


Figure 3. Schematic drawings for solid surface wetting phenomenon and their correlation with the limiting factors in water harvesting performance: a) determination of the contact angle on a flat

smooth solid surface that is hydrophilic ($\theta < 90°$); b) contact angle on a flat smooth solid surface that is hydrophobic ($\theta > 90°$); c) droplet pinned on the surface, large contact angle hysteresis; d) high droplet mobility, low contact angle hysteresis; e) Wenzel state: droplet impaled on the roughness features; f) Cassie-Baxter state: droplet rests on top of roughness features, with air trapped underneath.

Contact angle & Young's Equation [18], [20], [21], [22], [23]

The contact angle is a key characteristic of solid surface properties. The wettability of a solid surface is primarily governed by its surface chemistry, which dictates the balance of interfacial energies at the three-phase contact line (TPCL). TPCL is the boundary line where the solid surface, liquid droplet, and surrounding vapor meet, defining the local geometry that governs contact angle and droplet mobility. For a droplet of a liquid at a smooth homogeneous and inert solid-gas interface, the contact angle θ formed by the intersection of the surface of the droplet and the surface of the studied material is defined through Young's equation:

$$\cos\theta = \frac{\gamma_{SG} - \gamma_{SL}}{\gamma_{LG}}$$

γ_{SG} is the surface free energy for substrate/vapor interface. γ_{SL} and γ_{LG} are interfacial free energies of solid/liquid and liquid/vapor interfaces, respectively. The static contact angle is defined under ideal equilibrium conditions between the droplet and the solid surface without external perturbation. For partial wetting on hydrophilic surface, $0° < \theta < 90°$, the material has a surface free energy that satisfies the relation that $\gamma_{SG} > \gamma_{SL}$. A solid surface with high surface energy, such as clean metals or oxides, tend to lower γ_{SL}, leading to enhanced wetting and smaller contact angle. For non-wetting on hydrophobic surface, $90° < \theta < 180°$, the material satisfies the relation that $\gamma_{SG} < \gamma_{SL}$. Low energy, such as those modified with fluorochemicals or hydrocarbons, resist liquid spreading, leading to larger contact angle.

Contact Angle Hysteresis (CAH)

In practical systems, droplets rarely remain at equilibrium, and therefore, in addition to static contact angle described by Young's equation, a dynamic contact angle is also essential to characterize the surface wetting properties. The dynamic contact angle refers to the instantaneous angle observed when the contact line is in motion, which is advancing or receding. Contact angle hysteresis is the difference between the advancing and receding contact angle. Advancing is when the TPCL/interface is moving towards the vapor phase, whereas receding is when TPCL is moving away from the vapor phase.

$$CAH = \theta_{Adv} - \theta_{Rec}$$

The dynamic contact angle depends on external conditions such as droplet velocity, applied forces, or substrate inclination, and therefore often deviates from the static value. Such deviations are influenced by the surface roughness, chemical heterogeneity at the moving contact line. CAH reflects the wettability of rough surface, and is critical to adhesion, droplet mobility, and energy barriers to wetting states transitions. The observation of droplet pinning to the surface during condensation is usually reflected in large CAH, when the released surface energy upon droplet coalescence is not sufficient to overcome contact line pinning. [24]

Wenzel model

Wetting behavior on rough surface is important for many practical applications. Wenzel wetting is obtained on a rough but homogeneous substrate. It describes how surface roughness influences the solid surface wettability when a liquid completely penetrates the surface asperities. θ^* is the apparent contact angle on the rough surface, and it is related to the intrinsic contact angle θ on the smooth and chemically identical surface:

$$\cos\theta^* = r\cos\theta$$

where r is the roughness factor, defined as the ratio of the true surface area to its project area ($r \geq 1$). This relationship shows the surface roughness amplifies the intrinsic wettability of a surface: hydrophilic surfaces become more hydrophilic, while hydrophobic surfaces become more hydrophobic.

Cassie–Baxter model

On substrates that are highly textured and chemically heterogeneous, air entrapment often prevents complete liquid penetration, leading to a Cassie-Baxter state. Pockets of air become trapped beneath the droplet, resulting in a composite solid-liquid-air interface. The Cassie relation characterizes the local wetting at some point of the contact line. The roughness of the wetted surface causes the deviation of the measured contact angle from that on a smooth surface. The apparent contact angle θ^* in this wetting state with respect to the intrinsic contact angle θ is given by:

$$\cos\theta^* = f_s\cos\theta - (1 - f_s)$$

where f_s is the fraction of the solid surface in direct contact with the liquid. This relationship indicates the presence of trapped air can significantly increase the apparent contact angle. This also

explains how to achieve superhydrophobic surfaces ($\theta > 150$□) which exhibits properties such as self-cleaning (Lotus effect), reduced adhesion, and high droplet mobility.

The Cassie-Baxter wetting model is a metastable state, which can transition into the Wenzel wetting model under sufficient external pressure, vibration, or liquid infiltration. Both wetting models provide the theoretical foundation for tailoring surface wettability via hierarchical roughness and chemical patterning.

Experimental method for determination of CA for a sessile droplet on the surface

The sessile drop method is the most widely used and straightforward technique for CA measurement on a solid surface. A small liquid droplet is deposited onto the solid substrate, and its profile is imaged to determine the angle formed at the TPCL. The static contact angle is measured when the droplet is at rest under ambient conditions by a goniometer or optical tensiometer. The sessile drop method can be extended to measure advancing and receding contact angles to study the dynamic behavior of the contact line. To measure the advancing contact angle, liquid is added to the droplet until it reaches the maximum angle before the contact line begins to move outward. Conversely, the receding contact angle is measured by withdrawing liquid from the droplet until it reaches the minimum angle before the contact line retreats.

2.3.2 Droplet dynamics on surface

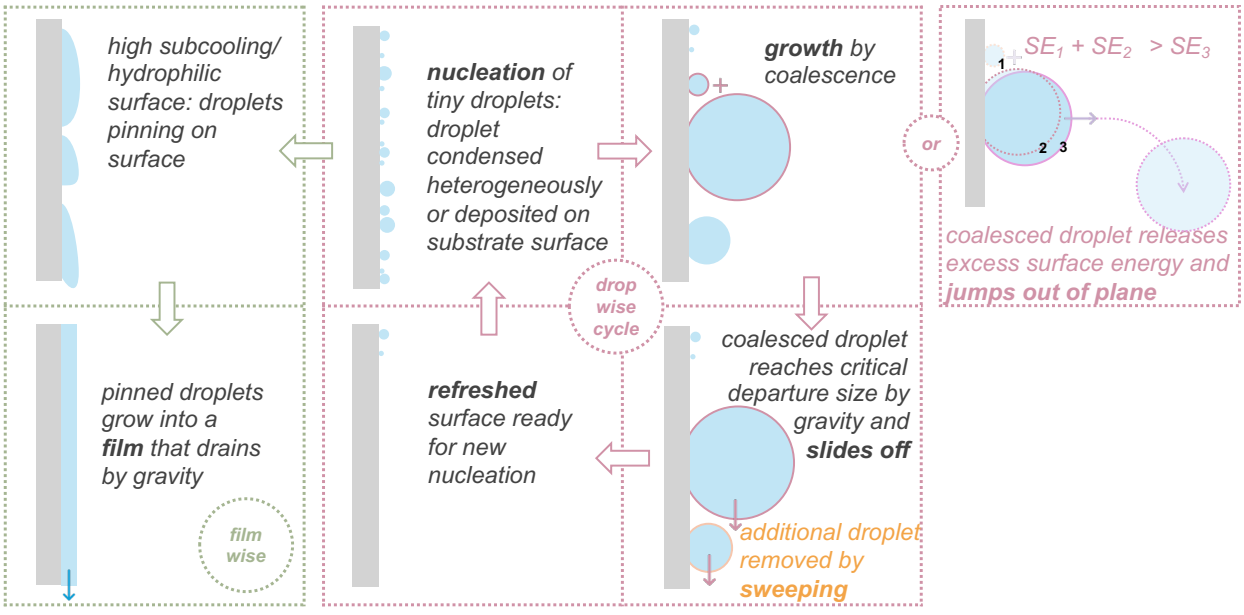


Figure 4. Schematic drawings of droplet nucleation, growth, and departure on vertically placed surface (side view) to illustrate dropwise and filmwise water drainage approach for fog and dew water harvesting.

To build surfaces with high water harvesting efficiency, it is crucial to first understand the droplet dynamics on the surface. Droplets undergo a cycle of nucleation, growth, and departure, which determines the extent to which the surface remains available for renewed condensation. In addition, unique phenomena such as coalescence-induced droplet jumping can dramatically influence water collection and transport efficiency.

Droplet nucleation, growth, and departure

Vapor condensation or droplet deposition begins with nucleation at favorable sites on a surface, often governed by surface energy.[25] On hydrophilic regions, nucleation occurs more readily, leading to a higher density of microscopic droplets, while hydrophobic regions delay nucleation but support mobility. Once formed, droplets grow either by direct vapor condensation or by coalescence with neighboring droplets. Over time, larger droplets either slide off, roll away, or remain pinned depending on their wetting states. In *filmwise* mode, the *pinned* droplets quickly coalesce into a continuous film, whereas in dropwise mode, droplets depart individually, continuously refreshing the surface for new nucleation. This cyclic renewal of nucleation sites is a key factor behind the superior efficiency of dropwise over filmwise condensation. [25]

Coalescence-induced droplet jumping

Beyond gravity-driven removal, coalescence-induced droplet jumping provides an additional pathway for droplet departure on superhydrophobic or specially engineered surfaces.[26] When two or more micrometer-sized droplets merge, the reduction in surface area leads to the sudden release of excess surface energy. This energy is converted into kinetic energy, propelling the coalesced droplet away from the surface in a "jumping" motion. The effect is most pronounced for droplets of similar size, where the coalescence event maximizes energy release. Jumping droplets can also collide with other droplets, inducing cascading coalescence events that rapidly clear a surface region. This autonomous removal mechanism minimizes droplet pinning, accelerates drainage, and ensures that condensation sites remain continuously active. However, the effectiveness of jumping is strongly dependent on environmental conditions: in humid air with high concentrations of non-condensable gases, diffusion limits can reduce droplet nucleation density, thereby lowering the frequency of coalescence events. [27], [28], [29] Together, these droplet dynamics—whether by gravity-driven shedding, surface sweeping, or coalescence-induced jumping—determine how effectively a surface can sustain dropwise mode. Designing surfaces that balance high nucleation density with efficient droplet departure mechanisms remains central to advancing the performance of atmospheric water harvesting systems.

2.3.3 Surface with patterned wetting properties

The advantage in both water capture and drainage

Surfaces with patterned wetting properties, where regions of contrasting or gradient wettability are arranged in controlled or random configurations, is one of the most common strategies in enhancing efficiency in AWH. Unlike uniformly hydrophobic or hydrophilic surfaces, the design of wetting patterns is targeted for simultaneously promoting droplet nucleation and water transport, overcoming the major trade-off in fog and dew harvesting systems. On such surface, hydrophilic domains reduce the energy barrier for nucleation and act as the preferential sites for nucleation for condensation or droplet deposition. This creates higher droplet density and earlier onset of water collection. The hydrophobic domains, with reduced contact angle hysteresis, facilitate droplet mobility by enabling coalesced droplets to roll or slide away by gravity. Such complementary interplay ensures water droplets are efficiently captured and continuously removed, quickly refreshing the surface for renewed cycle of condensation or droplet deposition. [30]

Inspired by the desert beetle's hydrophilic bumps on hydrophobic cuticle, dotted wettability pattern is one of the most common designs. The hydrophilic spots promote localized nucleation with a hydrophobic matrix that maintains droplet mobility. Alternating stripe or line pattern is another common design to guide coalesced droplets along defined channels towards a collection reservoir. In addition, a gradient pattern, where a surface gradually transitions from hydrophilic to hydrophobic, exploits Laplace pressure differences to drive the spontaneous droplet motion from hydrophilic zones (nucleation) towards hydrophobic zones (drainage). [31]

Fabrication methods

There are a variety of methods in the fabrication of such surfaces. Photolithography enables precise micro and nano scale definition of hydrophilic and hydrophobic domains. Laser surface texturing is a more flexible approach by locally altering surface chemistry to create wetting contrasts. Plasma treatment combined with masking is a relatively simple and scalable method that uses selective plasma exposure to create hydrophilic regions on otherwise hydrophobic surfaces. Chemical coatings and self-assembled monolayers are widely used to control selective wettability at the molecular level. Fluoropolymers and silanes are the common hydrophobic coatings. Lastly, 3D printing also known as additive manufacturing is a novel technique for fabricating complex biomimetic structures with integrated wettability contrast. Overall, these various types of methods have enabled significant laboratory advances. However, the critical challenge in employing such engineered surfaces in practical AWH applications remains in their scalability, durability, and cost.

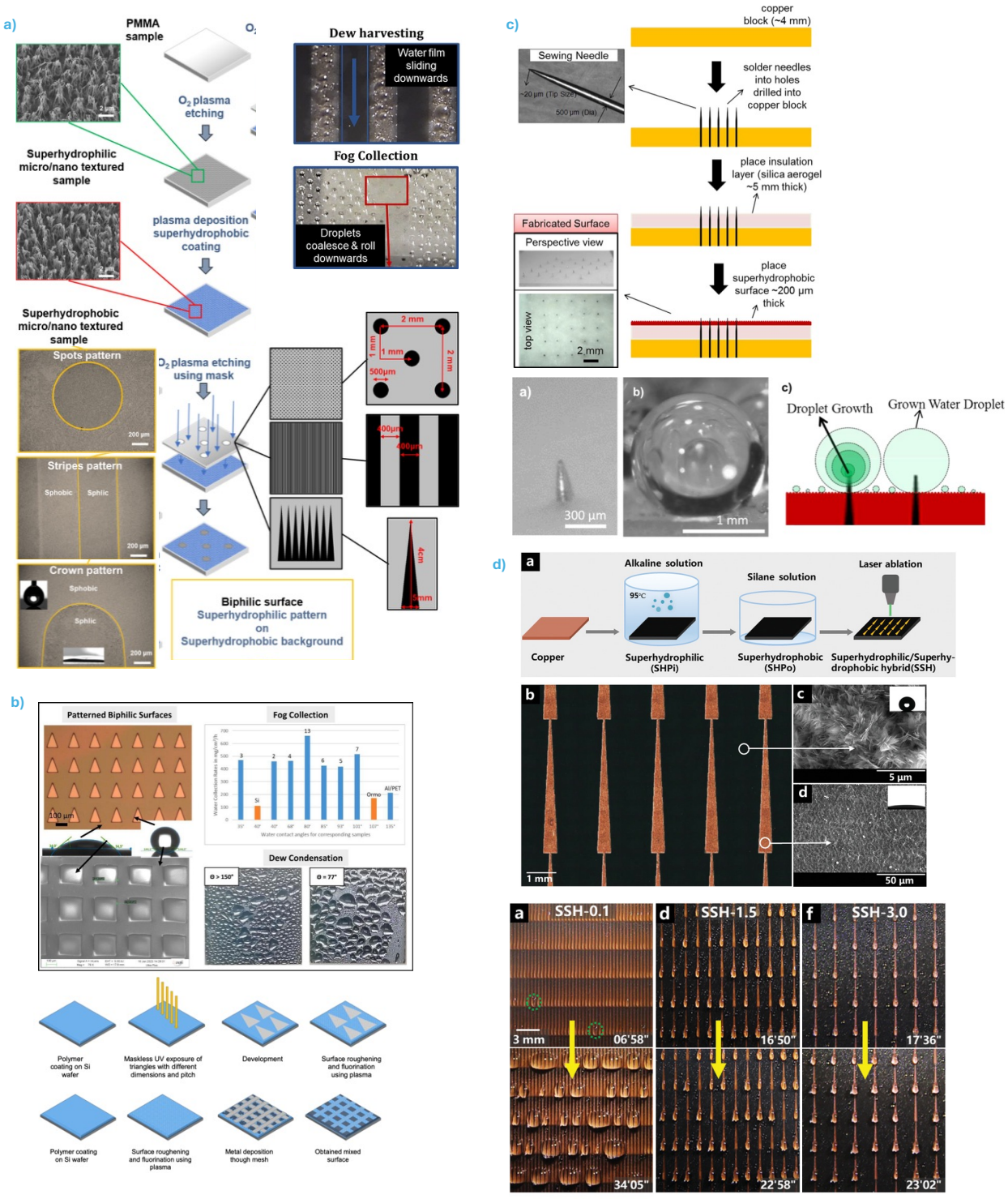


Figure 5. Surfaces with special design in wetting properties that enhance water harvesting performance: a) biphilic surface fabrication using plasma micro-nanotexturing, plasma deposition, and plasma etching through astencil mask; three biphilic patterns are tested both for dew and fog water harvesting (adapted from[32]); b) sample preparation using lithography and

metal deposition (adapted from [33]); c) hybrid superhydrophobic–hydrophilic surface: fabrication process and condensation observation; schematic of droplet growth due to preferential nucleation and droplet growth on the hydrophilic needle (adapted from [34]); d) fabrication process of the superhydrophilic superhydrophobic hybrid surfaces, optical image, SEM images, and CA of the laser treated and untreated area; dew water collection dynamics with 0.1, 1.5, and 3.0 mm spacing (upper image: droplet coalescence; lower image: droplet sliding off surface) (adapted from [35])

2.3.4 Surface with micro-nano structures

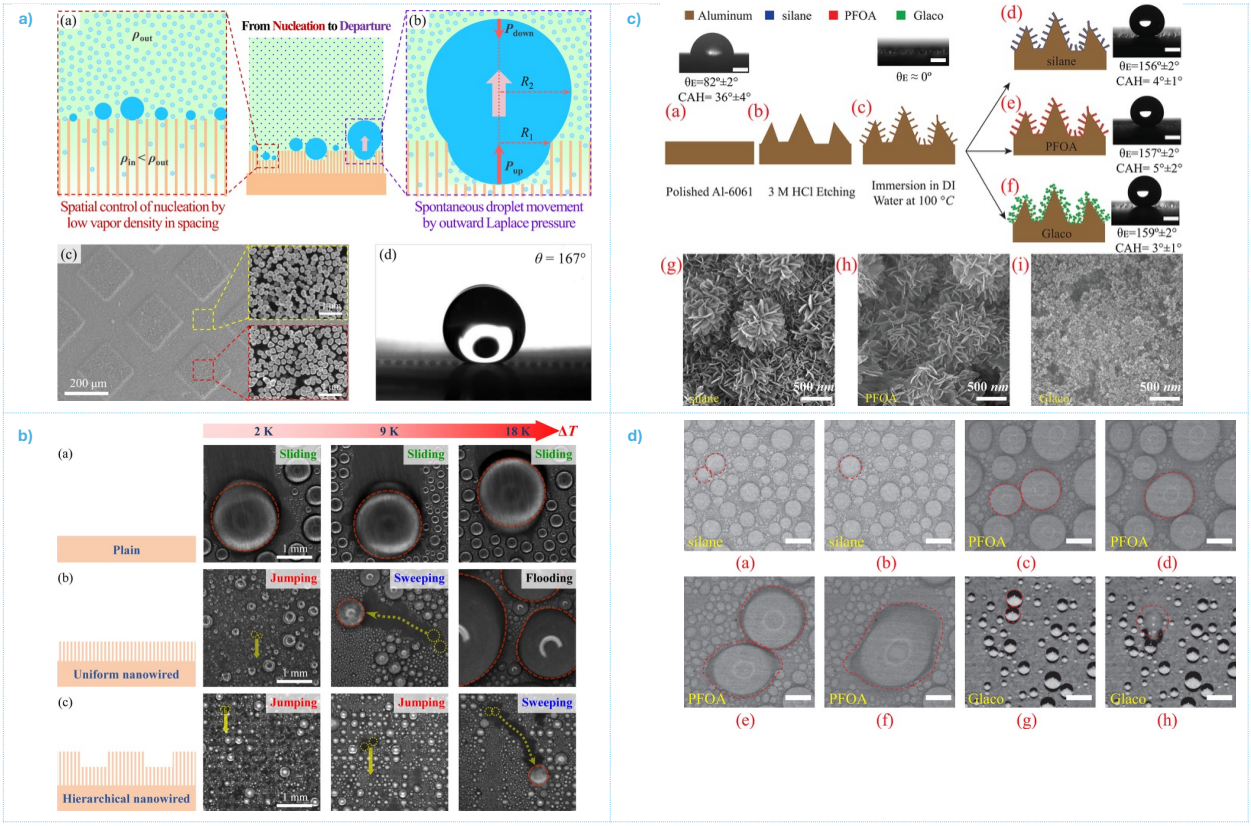


Figure 6. Surfaces with micro-nano structures: a) design of the hierarchical superhydrophobic surface with micropatterned nanowire arrays for the nucleation control and rapid departure of condensed droplets; b) Condensation modes and droplet behaviors on the three test surfaces under different surface subcooling (adapted from [36]); c) SEM and fabrication procedure of hierarchical surfaces with various nanocoatings; d) observation of droplet dynamics during condensation on different coatings (spherical Cassie droplets, pinned Wenzel droplets, and jumping droplets) (adapted from [27])

Plain, one-tier, and hierarchical roughness structure

In addition to creating wettability contrast on surfaces, another major strategy in enhancing efficiency in AWH is surface with micro and nano scale roughness. Surface texture influences

condensation and droplet transport by altering contact angle, droplet adhesion, and departure behavior. The tailoring of surface roughness across multiple length scales enables autonomous droplet departure and directional water transport.

Regular arrays of micro-pillars or micro-cones are the common features of rough superhydrophobic surfaces. The wetting states of droplets are Cassie-Baxter, which reduces contact angle hysteresis and improves droplet mobility. For capillary-driven pathways, nano-grooves and ridges enable directional droplet movement. Natural plant surfaces such as lotus leaves and desert moss possess a combination of microscale (such as pillars or ridges) and nanoscale (such as nanowires or nanogrooves) features to achieve surface superhydrophobicity or moisture extraction from air. [27] These surfaces with hierarchical micro-nano structures can be fabricated to have very high contact angles and low CAH macroscopically and exhibit different condensation behaviors by changes in its nanocoating chemistry.

2.4 Condensation mode and practical AWH design

2.4.1 DWC is the target for surface designs

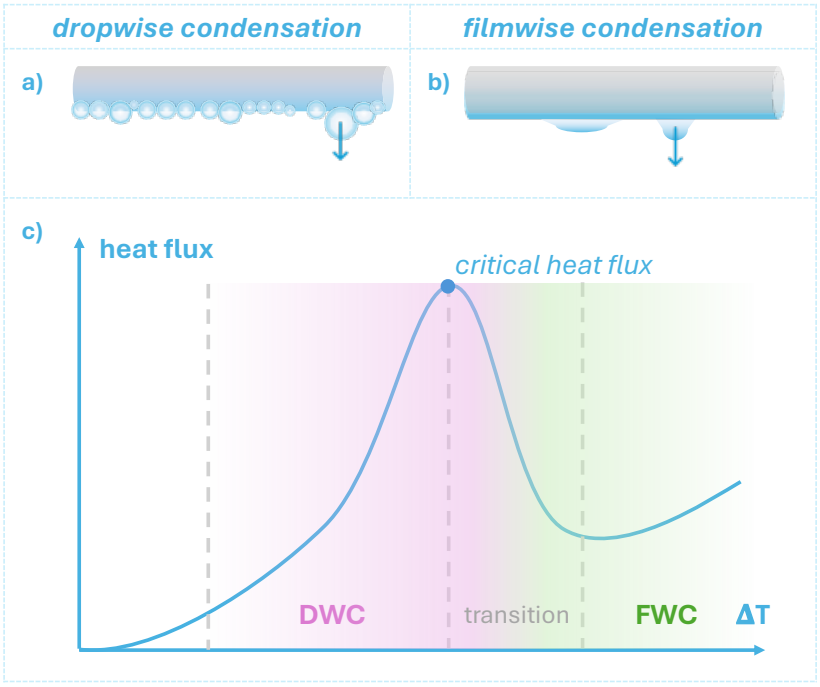


Figure 7. Schematics of condensation modes: a) dropwise: discrete droplets nucleate, grow, coalesce, and depart on the cooled surface of a tube; b) filmwise: continuous liquid film spreads over the cooled surface of a tube; c) heat flux plotted as a function of subcooling ($\Delta T = T_{surface} - T_{ambient}$), which shows the transition from dropwise to filmwise mode as the subcooling increases.

Condensation on solid surfaces generally occurs in two distinct modes: filmwise and dropwise. Numerous previous studies have demonstrated that DWC mode is much more efficient compared to the FWC mode, in that it has higher heat and mass transfer coefficient. DWC is characterized by discrete droplets that nucleate, grow and depart from the surface, refreshing the surface for a new cycle and therefore minimizing the condensate layer thickness. In contrast, in FWC, a continuous film forms across the surface, which creates a thermal resistance barrier to further condensation process, and is thus less desirable for applications involving condensation. [37]

DWC is widely regarded as the more efficient mode, with one order of magnitude higher in heat transfer coefficients than that of FWC mode under pure steam conditions, mainly due to the reduced conductive heat resistance through condensate films. DWC are commonly achieved on nanoengineered and chemically treated superhydrophobic surfaces that promotes the autonomous droplet departure mechanism, such as coalescence-induced jumping and gravity-assisted sweeping. [38], [39]

One reason that the less efficient FWC is still the major condensation mode in industrial applications is the difficulty in maintaining DWC mode under long-term operational conditions. Various studies have demonstrated that room temperature superhydrophobic surfaces can lose their superhydrophobic properties if the surface is subcooled. [40], [41], [42], [43] In addition, for higher degree of subcooling or longer subcooling time, DWC mode can transition into FWC mode. Despite these issues in practical applications, DWC consistently outperforms FWC in lab scale studies under pure vapor conditions, making it the preferred mode for designing surfaces for condensation-based systems.

2.4.2 The lack of comprehensive comparison for humid air condensation

The design of dew water harvesting devices need to first consider its ambient condition, which is atmospheric moisture. The air consists of more than 95 % non-condensable gases, and their presence may have an impact on the atmospheric moisture condensation process. This raises the question regarding whether the previous conclusion on DWC being the preferred condensation mode is still applicable for AWH applications.

Only few comprehensive studies or reviews specifically investigate the condensation performance of surfaces in atmospheric humid air conditions. The compilation and analysis of published literature results may not be sufficient in finding a possible correlation between surface wetting properties and their condensation efficiency. The previous subsection has shown that the ambient condition (relative humidity, air temperature, air flow) and device operating condition

(surface subcooling) both impact the condensation mode and performance. Each published result is impacted by these conditions. In addition, there are a lot of experimental uncertainties.

Attempting to prove the hypothesis that FWC may be the preferred mode in condensing atmospheric moisture for dew harvesting applications, Thomas et al. fabricated four surfaces with different wetting properties and compared their water collection performance under a wide range of ambient and operating conditions. Indeed, their results show that a superhydrophilic surface with micro and nano roughness produced the best result for all tested conditions. This observation is somehow contradictory to the previous widely demonstrated finding that DWC has higher heat and mass transfer efficiencies. To explain the results, they proposed a model that shows the formation of condensate liquid film is not the major contribution to heat resistance. And their study raised the interesting question of understanding the role of non-condensable gas (NCG) in the condensation process.

2.4.3 Role of non-condensable gases in condensation

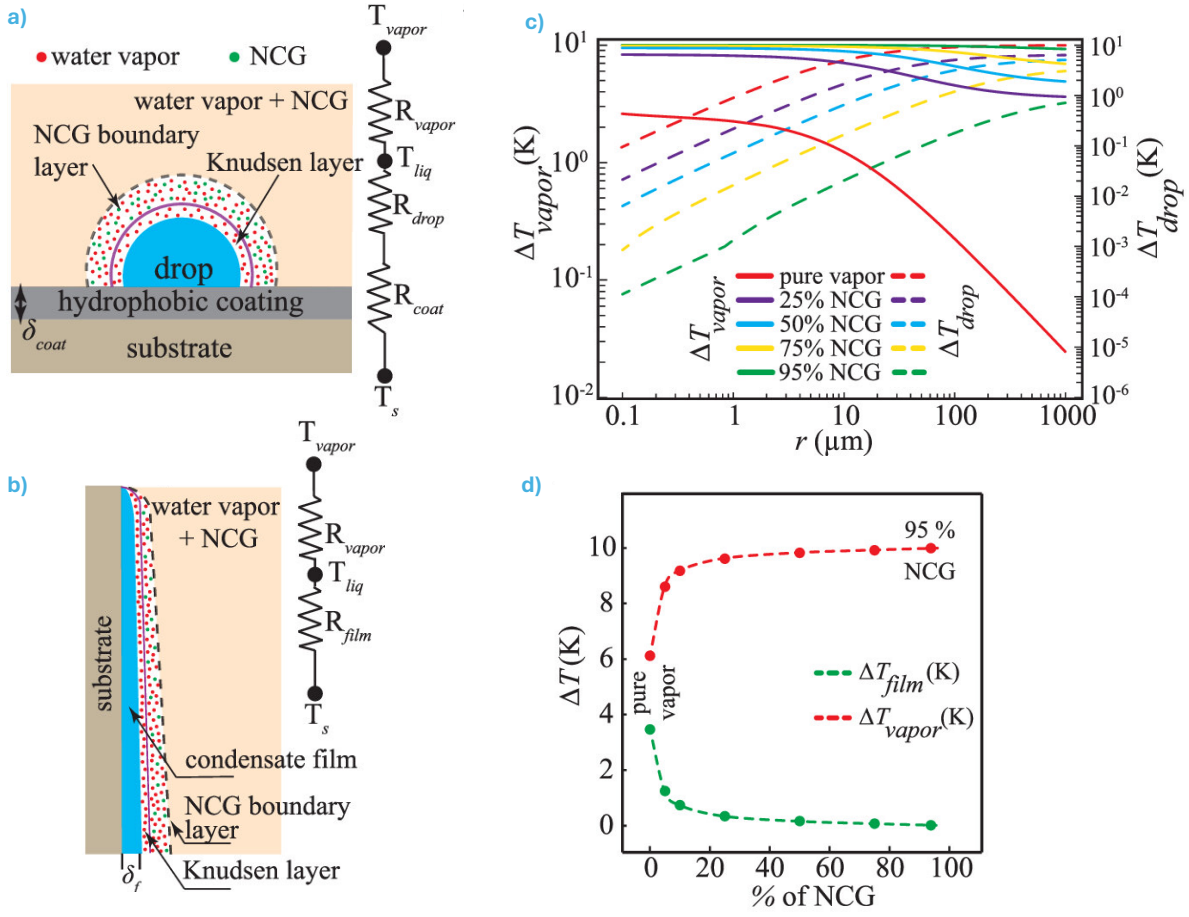


Figure 8. heat transfer models of vapor condensation in presence of NCGs for analysis of individual contribution of temperature drop: a) a droplet on superhydrophobic coating; b) a

condensate film; c) temperature drop across the vapor region d) temperature drop due to conduction (adapted from [44])

Non-condensable gases and reduced heat transfer

As early as the 1920s, Donald Othmer made a significant contribution to heat transfer research in condensation, particularly regarding the role of non-condensable gases.[45] His studies showed that the presence of small amounts (0.1 to 1%) of non-condensable gases (such as air) in vapor steam drastically reduces the overall heat transfer efficiency (by 30 to 90 %) during the condensation process. His work demonstrated the significance of diffusion resistance: NCG form a stagnant boundary layer at the condensing surface and cause the slow diffusion of vapor through this layer, in addition to the condensate film.

In practical conditions in AWH, water vapor only exists as part of the component in the atmospheric air. 95 % of air is NCG such as nitrogen, oxygen, and carbon dioxide. The presence of these NCG has a profound impact on condensation efficiency in the design of AWH systems. Rather than droplet dynamics dominating the condensation performance in the pure steam environments, the limiting factor in humid air condensation is the diffusion of vapor molecules through the stagnant boundary of NCG layer at the condensing surface. The diffusion resistance reduces the local vapor condensation and lowers the effective driving force for condensation, supressing both nucleation and growth of water droplets. Studies show that at high NCG concentrations, the heterogeneous nucleation rate can decrease by several orders of magnitude, with DWC being disproportionately affected compared with FWC. [45], [46]

In addition, the thermal resistance across the gas layer needs to be added to the overall heat transfer process. In presence of NCGs, the temperature drop across the vapor phase dominates the overall process, rendering the conductive resistance through condensate droplets, condensate films, or surface coating relatively negligible.

Understanding and accounting for the influence of NCG is critical in the design of engineered surface for AWH systems. Therefore, the strategies overcome this challenge should focus on optimizing surface wettability to enhance nucleation and droplet mobility. The NCG-induced diffusion resistance remains one of the primary barriers to developing and scaling condensation-based AWH systems in real-world environments.

Condensation mode and water collection in presence of NCG

As the presence of NCG is a major factor that degrades condensation efficiency, it is worth further investigation how DWC and FWC mode are each impacted. The relative performance

advantage of DWC under pure steam conditions may no longer be the case for humid air condensation for AWH systems. In FWC, the continuous liquid layer already imposes thermal resistance, and the presence of NCGs exacerbates this by impeding vapor diffusion through the gas boundary layer. This finding underscores the challenge of sustaining high-performance DWC in realistic atmospheric environments.

Recent work has attempted to quantify and model these effects. Semi-empirical and theoretical approaches, including diffusion layer and boundary layer models, have been developed to predict condensation mass flux under varying NCG concentrations. Poredoš et al showed that empirical correlations could be adapted for different geometries, such as vertical plates and horizontal tubes. [46] Meanwhile, Huang et al emphasized that the dominant mechanisms include condensate film thickness, interfacial shear, and surface waves, all of which interact with NCG distribution. [45] Together, these findings confirm that overcoming NCG-related resistance is one of the most critical bottlenecks in advancing condensation-based atmospheric water harvesting systems.

2.5 Summary and implication for current project

The literature reviewed above demonstrates that surfaces with special chemical and structural characteristics provide an innovative and sustainable pathway to harvest fog and dew water. Water collection efficiency of a surface is fundamentally governed by its chemistry, topography, and wettability. The critical question that recent studies try to address is balancing the trade-off between nucleation density and liquid water removal for a surface to efficiently harvest water under varying environmental conditions. Despite the fundamental difference in the mechanism (surface-mediated droplet capture vs. heterogeneous vapor condensation on surface), fog and dew harvesting are both constrained by this same question. This review uses wetting theory to clarify the limitation in existing fog and dew water harvesting technologies, highlights the strategy of surface design in mixed wettability and micro-nano structures inspired from nature (desert beetle and moss), and further discusses the efficiency of dropwise and filmwise mode and the significance of non-condensable gases. However, there is still much future work in systematically understanding how to tailor surface characteristics to optimize water collection under varying practical conditions, and addressing the challenge in durability, scalability, and cost-effectiveness.

For the current project, these literature findings emphasize the importance of designing a surface that achieves a synergistic balance between water capture and drainage, while also being sustainable and robust under outdoor conditions. Cellulose nanocrystal-coated wax microparticles

made from Pickering emulsion is a good material to understand wettability and topography control in dew and fog water harvesting performance and has the potential to contribute to the understanding of droplet dynamics and overall water yield.

Chapter 3 CNC-coated Wax Microparticles: Variation in Synthesis Formula

3.1 Introduction

This chapter studies the sustainable surface materials with tunable wettability and surface structures, focusing on cellulose nanocrystal (CNC)-coated wax microparticles as the building block of surface coating. In this work, CNC is both used as the particle stabilizer for Pickering emulsion and the surface modifier imparting hydrophilicity, roughness, or hierarchical structures.

CNC have attracted significant attention as sustainable nanomaterials derived from lignocellulosic biomass. CNCs exhibit good mechanical strength and colloidal stability due to their high crystallinity, aspect ratio, and surface hydroxyl groups that can be chemically functionalized. [47], [48], [49] These features allow CNCs to be an excellent stabilizer for Pickering emulsions, where particles adsorb at the oil-water interface to prevent droplet coalescence and provide long-term emulsion stability (Figure 9). Compared with conventional surfactants, CNCs can form more robust interfacial layers, leading to tunable properties of the emulsion. [50], [51]

The CNC-stabilized Pickering emulsion is a versatile platform for developing functional particles, capsules, and coatings. The emulsion particles have a hydrophobic core and a CNC-coated shell. Their properties, such as size, morphology, and wettability, are tunable by adjusting the formulation during the emulsion synthesis process. Factors such as CNC concentration and oil-to-water ratio can have direct impact on the CNC interfacial coverage, droplet size distribution, and emulsion stability.[50], [51] Thus, careful control of synthesis formulation allows for systematic tuning of emulsion particle properties.

The incorporation of wax into CNC-stabilized Pickering emulsions adds new opportunities for fabricating microparticles with hydrophobic core and tunable surface functionality. Such hybrid material has a wide potential application, such as in sustainable coatings and controlled release. And therefore, a detailed understanding on the correlation between formulation parameters and CNC-coated wax particles properties would be the foundation for further applications. This work aims at coating that exhibits special wettability to promote fog and dew water harvesting performance.

This chapter discusses the synthesis of CNC-coated wax microparticle in Pickering emulsion and provides fundamental insights into the emulsion formulation parameters and the resulting emulsion properties. A series of factors, including CNC dispersion concentration, oil-to-water ratio,

ionic strength, and the incorporation of additional surfactant octadecylamine, are controlled for a systematic investigation on particle formation and emulsion stability. The ideal formulation is selected for the next step of coating performance evaluation in Chapter 4.

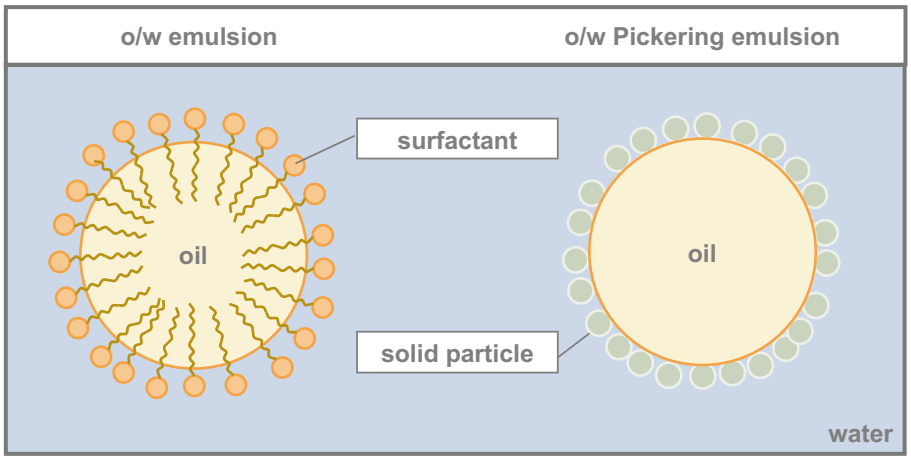


Figure 9. Schematic drawing of oil in water emulsion particle stabilized by surfactants vs. Pickering emulsion particle stabilized by solid particles

3.2 Experimental

3.2.1 Raw materials

Cellulose nanocrystals (Celluforce, Inc.), paraffin wax (Sigma-Aldrich), sodium chloride (Sigma-Aldrich), octadecylamine (Sigma-Aldrich), ethanol (Sigma-Aldrich), 37% hydrochloric acid (Sigma-Aldrich). All chemicals were used without additional purification, unless stated otherwise. Milli-Q water (resistivity of 18.2 MΩ·cm) was used to prepare the aqueous dispersions and solutions. All emulsions were made in glass scintillation vials (7 and 20 mL) pre-washed with Milli-Q water and oven dried.

3.2.2 Emulsion synthesis procedure

Stock solution preparation

CNC aqueous dispersions with different concentrations (0.1 to 3 g CNC/100 g aqueous dispersion) were prepared by dispersing pristine CNC powder in Milli-Q water followed by ultrasonic treatment for 2 h. NaCl aqueous solutions (0.05 to 1 g NaCl/ 100 g solution) were prepared by dissolving NaCl in Milli-Q water. Octadecylamine (ODA) ethanol solution (5 g ODA/ 100 g solution) was prepared by dissolving ODA in ethanol. HCl (1 M) was prepared by diluting 37% HCl in Milli-Q water.

CNC and NaCl formulation

Solid paraffin wax, CNC aqueous dispersion, and NaCl were added to the vial at room temperature. The mixture was placed in water bath at 70 °C. After solid wax was melted into liquid, the mixture was homogenized using the ultrasonic probe (Misonix-Microscon-XL2000) for 30s. The homogenized emulsion was allowed to cool at room temperature.

CNC and ODA formulation

ODA ethanol solution was added to solid paraffin wax, and the mixture was heated until the wax was melted. 1 M HCl was added to stock CNC dispersion to adjust pH to 3. The wax and CNC dispersion were added to the vial. The emulsion homogenization followed the same procedure as the CNC and NaCl formulation.

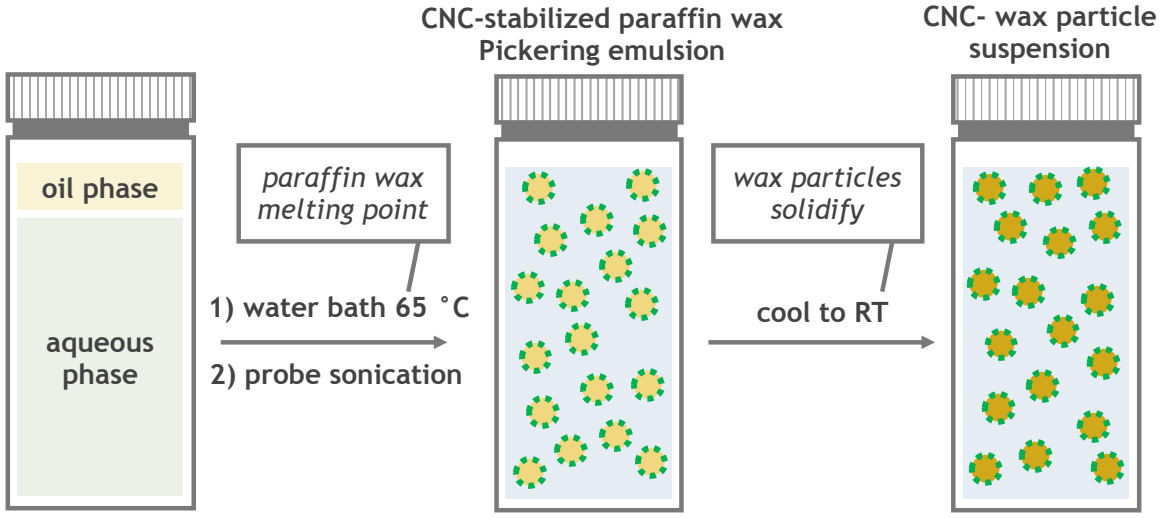


Figure 10. Synthesis procedure of CNC-coated solid wax microparticle suspended in water

Table 1. CNC-coated wax Pickering emulsion formula

	amount	salt formulation	surfactant formulation
oil phase component			
paraffin wax	5 to 25 wt% of emulsion	✓	✓
ODA	0.5 to 3 wt% in wax		✓
aqueous phase component			
water	75 to 95 wt% of emulsion	✓	✓
CNC	0.1 to 3 wt% in water	✓	✓
NaCl	0.05 to 1 wt% in water	✓	
HCl	adjust pH to 3		✓

3.2.3 Emulsion characterization

Particle size measurement

The particle size was measured using the particle size analyzer (Anton Paar 1190). For o/w CNC-stabilized paraffin wax Pickering emulsions, the particle size was measured at room temperature, where paraffin wax is a solid.

Zeta potential measurement

The zeta potential was measured using Nano Zetasizer (Malvern ZS90) with temperature control system.

3.3 CNC and NaCl formulation

In Pickering emulsion synthesis, the behavior of CNC is strongly influenced by the ionic environment. Salt ions play a crucial role in modulating CNC surface charge through electrostatic screening, which alters dispersion stability and interfacial adsorption. Understanding this salt–CNC interaction is essential for controlling emulsion formation, droplet size, and stability, as it determines how effectively CNCs can assemble at the oil–water interface.

3.3.1 Ionic strength and CNC aggregation in aqueous dispersion

Figure 10 schematically shows the synthesis of wax microparticle suspension from Pickering emulsion. Table 1 shows the compounds dispersed or dissolved in either oil or aqueous phase before homogenization. As pristine CNC exist as highly charged colloids in water, the environment of the aqueous phase critically determines their dispersion behavior and surface activity. The first objective is to understand how ionic strength (indicated by NaCl concentration) affects CNC dispersion stability and aggregation behavior, which directly influences the emulsion stability in subsequent steps.

For 1 wt% CNC dispersed in NaCl solution of various concentration (0 to 170 mM), there is a visual trend of turbidity change shown in Figure 11a. As NaCl concentration increases, the mixture changes from transparent to milky, suggesting there exists a threshold of ionic concentration where aggregation becomes significant. The zeta potential measurement (Figure 11b) shows a steady reduction in surface charge as NaCl concentration increases, reflecting progressive electrostatic screening of CNC sulfate groups. As pristine CNCs from acid hydrolysis carry negative surface charges due to the sulfate ester groups, the positive charges on sodium ions supress the electrical double layer, reducing the electrostatic repulsion between CNCs. For high ionic strength, CNCs start to aggregate due to the enhanced van der Waals attraction. Therefore, moderate screening is

required for the stabilization of Pickering emulsion with CNCs, while excess screening leads to CNC bulk aggregation.

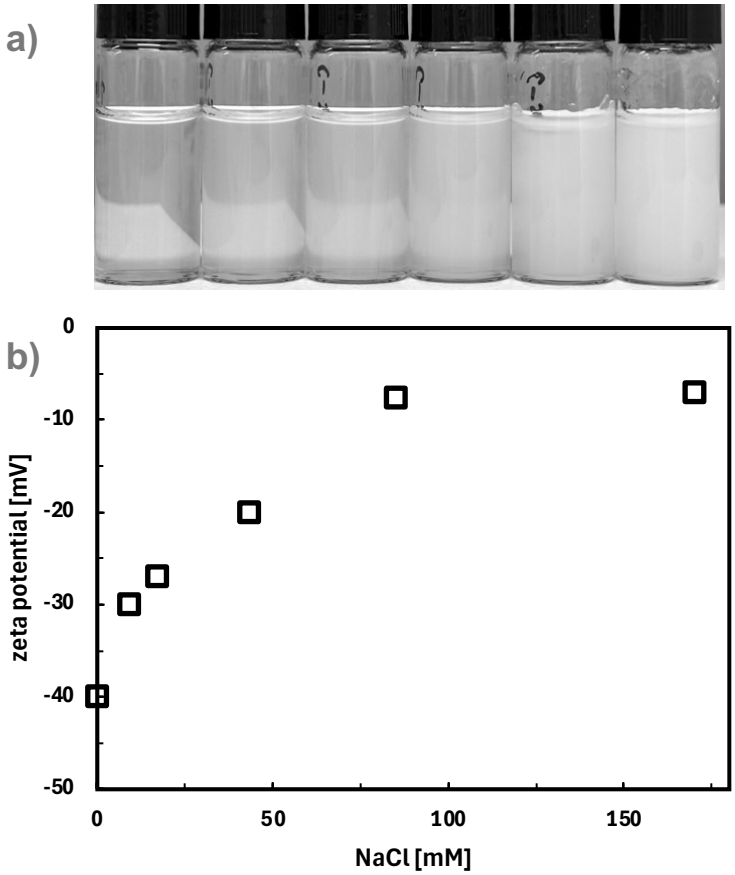


Figure 11. 1 wt% CNC dispersed in different NaCl solution (left to right: 0, 9, 17, 43, 85, 170 mM NaCl): a) picture of dispersion; b) zeta potential measurements.

CNC with different salt screening levels were used in the synthesis of o/w Pickering emulsion. No phase separation was observed for the synthesized emulsion stored at 80°C for up to one week, indicating salt-screened CNC is effective in stabilizing liquid paraffin wax. In contrast, pristine CNC and wax only emulsion quickly phase separate after synthesis and cannot be used as surface coating. As the salt-screened CNC stabilized Pickering emulsion cools down to RT, wax particles solidify and form a suspension. Figure 12a and 12b shows the visual trend of suspension (diluted to 5 wt% solid content) made from different salt concentration (9, 17, 43, 85, and 170 mM). For 0.5 wt% CNC, the suspension exhibits clear changes with increasing NaCl concentration. At low salt levels, the suspension is opaque and homogeneous, suggesting well-dispersed wax particles stabilized by a sufficient electrostatic barrier. As NaCl concentration increases to intermediate levels

(50–100 mM), partial flocculation and network formation become evident, resulting in thicker upper layers and an increasingly defined lower aqueous layer. At high ionic strength (≥150 mM), a pronounced upper wax-rich layer forms, while a clear lower aqueous layer appears. This is not true phase separation but rather creaming, driven by the density difference between the solid wax particles (less dense than water) and the aqueous medium. The loss of uniform dispersion is attributed to excessive charge screening, which diminishes interparticle repulsion and allows aggregation into larger clusters that cream more rapidly. For 1 wt% CNC, similar trends are observed but the suspensions show greater tolerance to ionic strength variation.

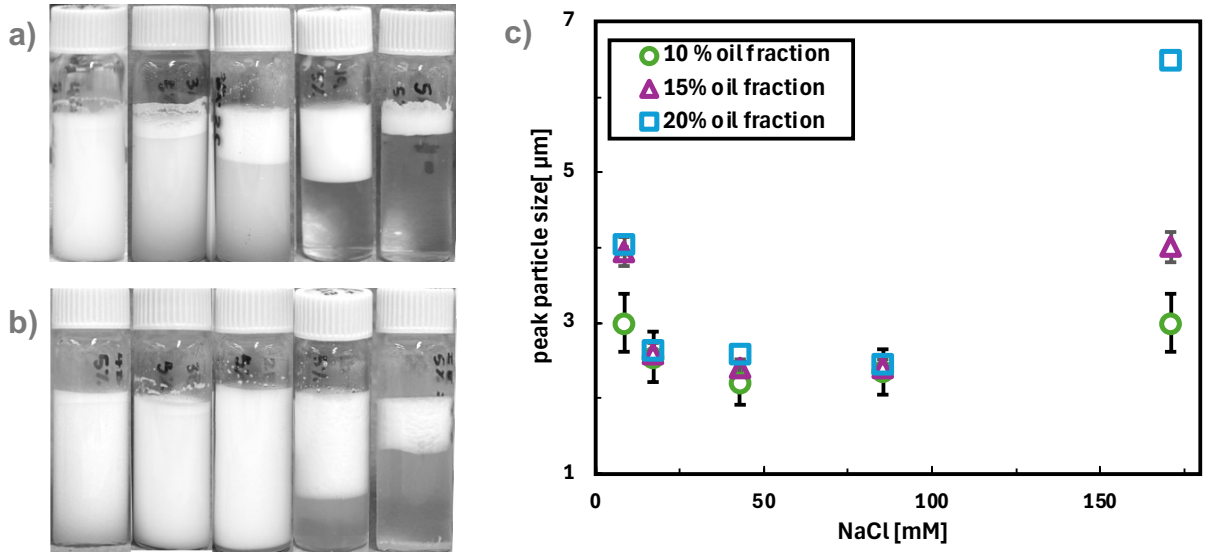


Figure 12. CNC-coated wax microparticle suspensions: a) pictures of 5 wt% solid content suspension (synthesis formula: 0.5 wt% CNC in varying NaCl solutions, 10% oil fraction); b) pictures of 5 wt% solid content suspension (synthesis formula: 1 wt% CNC in varying NaCl solutions, 10% oil fraction); c) peak particle size measurement (synthesis formula: 1 wt% CNC in varying NaCl solutions, 10% to 20% oil fraction). Error bars represent the standard deviation across independently prepared samples of the same formulation. No replicates were done for the 20% oil fraction series.

Figure 12c plots the peak particle size of CNC-coated wax solid particle synthesized following formulation of varying NaCl concentration. In general, for all oil fractions, the relationship exhibits a U-shaped trend. The droplet size decreases initially with increasing salt concentration, reaching a minimum at approximately 25–50 mM NaCl, followed by an increase at higher ionic strengths (>100 mM). This characteristic behavior reflects the dual effect of ionic strength on CNC colloidal interactions and interfacial adsorption efficiency. At intermediate salt concentrations, electrostatic screening compresses the electrical double layer, lowering the repulsive barrier and

allowing CNCs to approach and adsorb efficiently at the oil–water interface. This enhances droplet stabilization by forming compact interfacial layers. The droplet size reaches a minimum (~2–2.5 μm) under these conditions, corresponding to optimal interfacial packing and stability. At high NaCl concentrations, excessive charge screening reduces the zeta potential magnitude ($\zeta \approx -20$ mV or less), leading to diminished electrostatic repulsion and enhanced van der Waals attraction. CNCs begin to aggregate in the bulk and at the interface, resulting in irregular adsorption and droplet coalescence. Consequently, the mean droplet size increases sharply, especially for the 15% and 20% oil fraction emulsions where CNC coverage per interface is more limited.

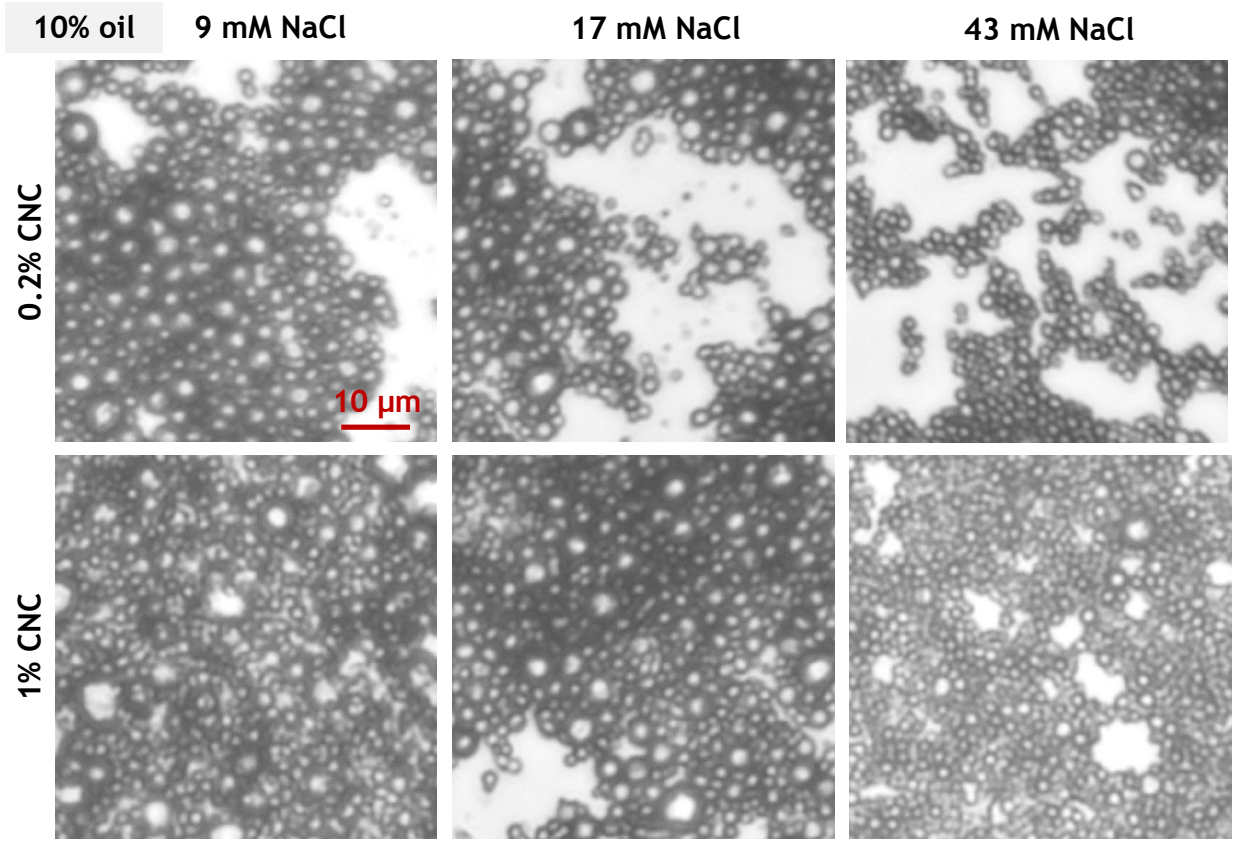


Figure 13. Optical microscopy images of CNC-coated wax microparticles (salt formulation, varying CNC and NaCl concentration)

Figure 13 shows optical microscopy images of the wax microparticles prepared using the salt formulation at 10% oil. Across all images, spherical wax droplets are observed, confirming successful emulsification and solidification of the dispersed phase. The particle size distribution and spatial organization vary noticeably between formulations. Some conditions exhibit relatively dense, closely packed populations of microparticles with a broad range of diameters, while others show more open structures with visible voids and clustering. These qualitative differences indicate that

changes in CNC and ionic strength significantly influence droplet breakup and stabilization during emulsification, affecting both the mean particle size and the uniformity of the distribution.

In formulations displaying more homogeneous packing, the particles appear smaller and more uniformly distributed, suggesting enhanced interfacial stabilization by CNCs under favorable salt conditions. In contrast, images with pronounced aggregation and wider size distributions likely result from insufficient electrostatic stabilization or partial CNC flocculation at higher or lower NaCl concentrations, leading to droplet coalescence during processing. The presence of larger particles and irregular clusters in these cases implies reduced emulsion stability prior to solidification. Overall, the optical microscopy results also shows the role of salt screening effects in controlling microparticle size distribution and structural uniformity.

Based on the visual observation of the wax suspensions and the trend in particle size, a moderately salt-screened system (43 mM NaCl) is selected for further formulation study so that CNCs retain partial surface charge while exhibit sufficient mobility to adsorb at the interface, creating an optimal balance between electrostatic repulsion and interfacial anchoring.

3.3.2 CNC concentration in aqueous dispersion

While discussed above in 3.2.1 that interactions among CNCs are modulated by the surface functional groups and ionic environment, it is the CNC concentration that governs how effectively CNCs the oil–water interface. To form stable Pickering emulsion, CNC irreversibly adsorbs at the oil–water interface, forming a steric–electrostatic barrier that prevents droplet coalescence. Figure 13a shows the visual trend of suspension (diluted to 5 wt% solid content) made from varying CNC concentration (0.2, 0.5, 1, 1.5, 2 wt%) The visual changes in opacity, homogeneity, and creaming behavior provide direct evidence of how CNC concentration influences the formation, packing, and stabilization of wax particles. As they are under the same moderate salt screening conditions (43 mM NaCl), all suspensions are relatively opaque and uniform, with only the lowest CNC concentration (0.2 wt%) exhibiting a visible creaming top layer and clearer aqueous layer. At this salt level, moderate electrostatic screening promotes CNC adsorption without inducing aggregation. The interparticle repulsion is sufficiently reduced to allow CNC to anchor strongly to the oil–water interface while maintaining colloidal stability in the continuous phase. As a result, the suspension remains opaque (indicating well-dispersed wax particles) and shows minimal creaming. For moderate and higher CNC concentration (0.5 wt% and above), the suspension is more homogeneous, indicating better stabilization, as the number of CNCs available per wax particle is sufficient to fully coat particle surfaces with dense CNC layers.

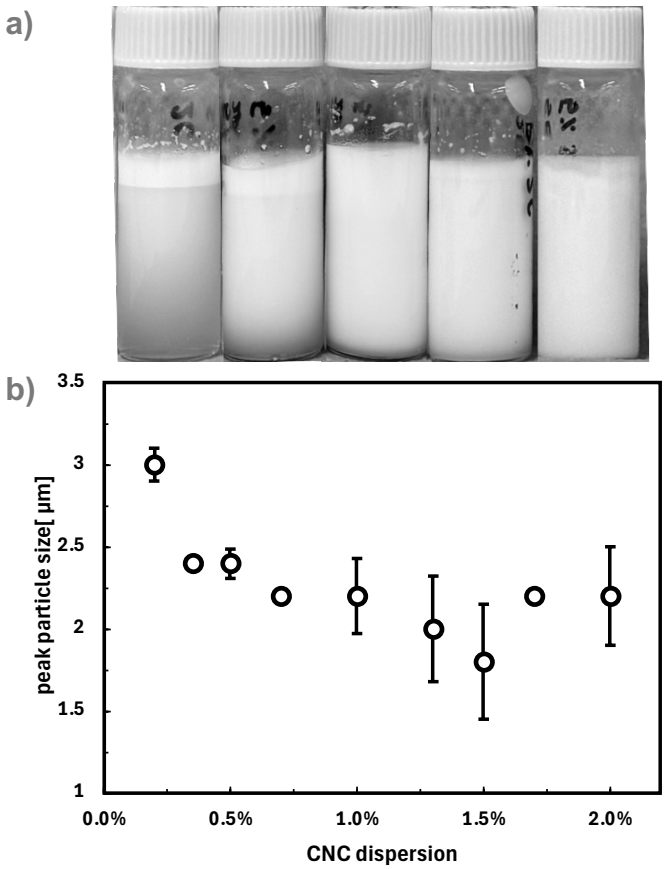


Figure 14. CNC-coated wax microparticle suspensions (synthesis formula: varying concentration of CNC dispersion in 43 mM NaCl solutions, 10% oil fraction): a) pictures of 5 wt% solid content suspension; b) peak particle size measurement. Error bars represent the standard deviation across independently prepared samples of the same formulation. No replicates were done for the 0.35%, 0.7%, and 1.7% CNC.

Figure 13b plots the peak particle size of CNC-coated wax solid particle synthesized following formulation of varying CNC concentration. In moderately ionic environments where the electrical double layer around CNCs is partially compressed, at low CNC concentrations (0.1 wt%), the available particle surface area is less sufficient to fully cover the growing oil droplets during emulsification. Only a fraction of the droplet surfaces is stabilized, leaving some uncovered regions prone to coalescence. The resulted wax suspension exhibits large droplet diameters, low viscosity, and rapid phase separation.

As the CNC concentration increases (0.2–0.5 wt%), interfacial coverage improves substantially. CNCs are more abundant, enabling rapid adsorption during emulsification and formation of dense particle shells around droplets. The droplet size decreases and the size

distribution narrows. Within this range, emulsions exhibit long-term stability and resist coalescence, demonstrating an optimal CNC concentration for Pickering stabilization.

Beyond 0.5–1.0 wt%, the system enters a particle-rich regime. The oil–water interface becomes saturated, and excess CNCs remain dispersed in the continuous phase, where they interact to form a weak percolated network. This network increases viscosity and sometimes induces gel-like behavior. While such systems remain stable, further increasing CNC concentration (>1 wt%) yields diminishing returns on droplet size reduction and can impede emulsification efficiency due to high bulk viscosity.

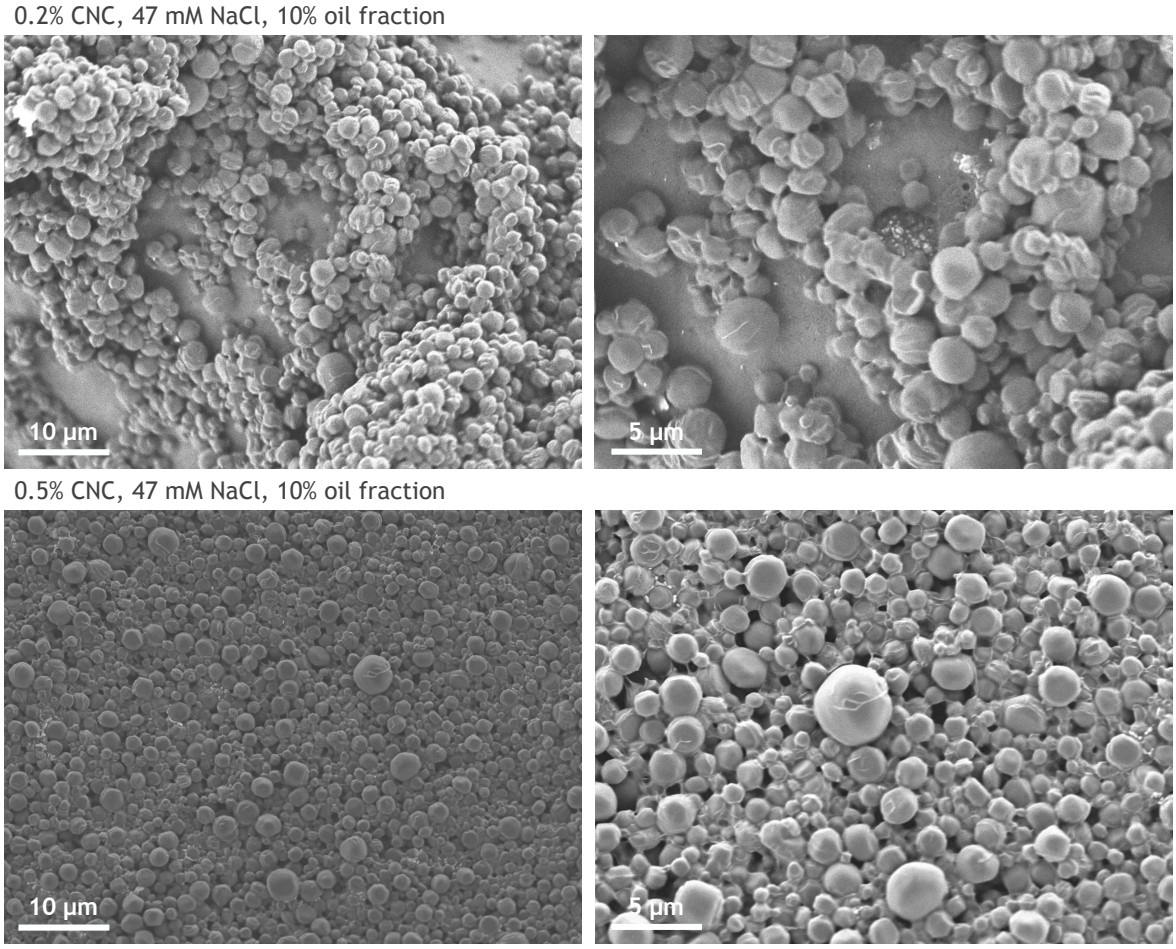


Figure 15. SEM images of CNC-coated wax microparticles (salt formulation)

The SEM images (Figure 15) compare the wax microparticles prepared at a with different CNC concentration. At 0.2% CNC, the particles exhibit pronounced aggregation and the formation of irregular clusters, with individual microparticles appearing partially fused or closely adhered. The surface coverage is non-uniform, and a broad particle size distribution is evident, with smaller

particles decorating the surfaces of larger ones. This morphology suggests limited interfacial stabilization during emulsification, where the available CNC content may be insufficient to fully cover newly formed oil–water interfaces, leading to droplet coalescence and post-solidification aggregation.

In contrast, increasing the CNC concentration to 0.5% results in a more uniform and densely packed population of spherical microparticles. The particles appear better separated, with smoother outlines and a narrower apparent size distribution, indicating improved emulsion stability prior to solidification. The higher CNC availability likely enhances interfacial adsorption, suppressing coalescence and yielding more consistent particle sizes. Overall, the SEM images demonstrate that increasing CNC concentration plays a critical role in controlling particle morphology, aggregation behavior, and size uniformity. This also corroborates with trends observed in optical microscopy and particle size distribution analyses.

Based on the visual observation of the wax suspensions and the trend in particle size, a moderate CNC dispersion concentration (0.5 to 1 wt%) is selected for further formulation study.

3.3.3 Oil phase fraction

After an investigation into the effect of ionic strength and CNC concentration, the last fundamental design parameter in the Pickering emulsion formula is the oil fraction. It directly determines the interfacial area available for stabilization and, consequently, the efficiency of particle adsorption at the oil–water interface. For the synthesis of CNC-coated wax microparticles, the oil fraction influences not only droplet size and distribution but also rheological behavior and long-term stability of the coating.

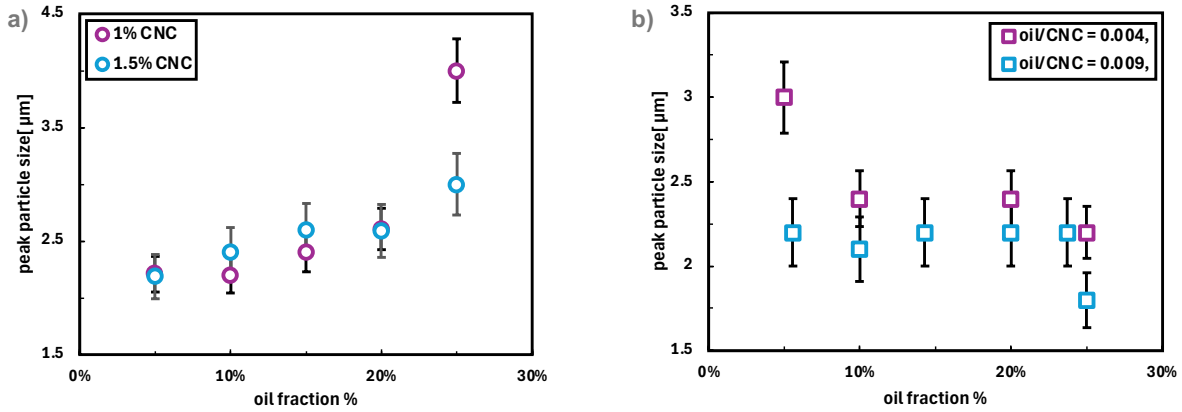


Figure 16. peak particle size measurements of CNC-coated wax microparticle suspensions. synthesis formula: a) 1 and 1.5 wt% CNC in 43 mM NaCl solutions, varying oil fraction; b) constant CNC to oil mass ratio, 43 mM NaCl solutions, varying oil fraction. Error bars represent

the relative error (relative errors of 1% and 1.5 %CNC, 43 mM NaCl, 10% oil fraction were measured from independently prepared samples, and were assumed to be the same for all oil fractions)

Two different formulation set were tested. In the first formulation set, the CNC concentration in the aqueous phase is kept constant while varying the oil fraction between 5 wt% and 25 wt%. At low oil fractions (5–10%), the available CNCs exceed the amount required for complete interfacial coverage, leading to the formation of small droplets. As the oil fraction increases, the interfacial area demand outpaces the fixed CNC availability. Consequently, droplets experience partial surface coverage, promoting droplet–droplet coalescence during and after emulsification. At the highest tested fraction (25%), phase separation appears when the emulsion is stored above the paraffin wax melting point. The emulsion becomes visibly unstable, exhibiting coalesced droplets and a significant decrease in overall homogeneity.

In the second formulation set, the CNC mass is scaled proportionally to the oil mass to maintain a constant CNC-to-oil ratio across all compositions. This ensures that, as the oil fraction increases, an equivalent increase in CNCs maintains the interfacial coverage fraction near unity. Under these conditions, stable emulsions are obtained throughout the 5–25% oil range. The droplet size in these emulsions remains relatively constant and the size distribution is narrow. The emulsions stored above the paraffin wax melting point remain stable over extended periods, demonstrating that sufficient CNC availability is the primary determinant of long-term stability under moderate ionic strength.

The contrasting outcomes of the two formulation strategies highlight the interdependence between oil fraction, interfacial area, and CNC availability. At 43 mM NaCl, the partial screening of CNC surface charge enhances interfacial adsorption, but the magnitude of stabilization still depends primarily on the number of CNCs present. The presence of excess salt alone cannot compensate for under-coverage at high oil fractions, as the stabilizing barrier against coalescence is mechanical and steric rather than purely electrostatic. This confirms that interfacial coverage, governed by the CNC-to-oil ratio, is the key controlling factor for emulsion stability under these conditions.

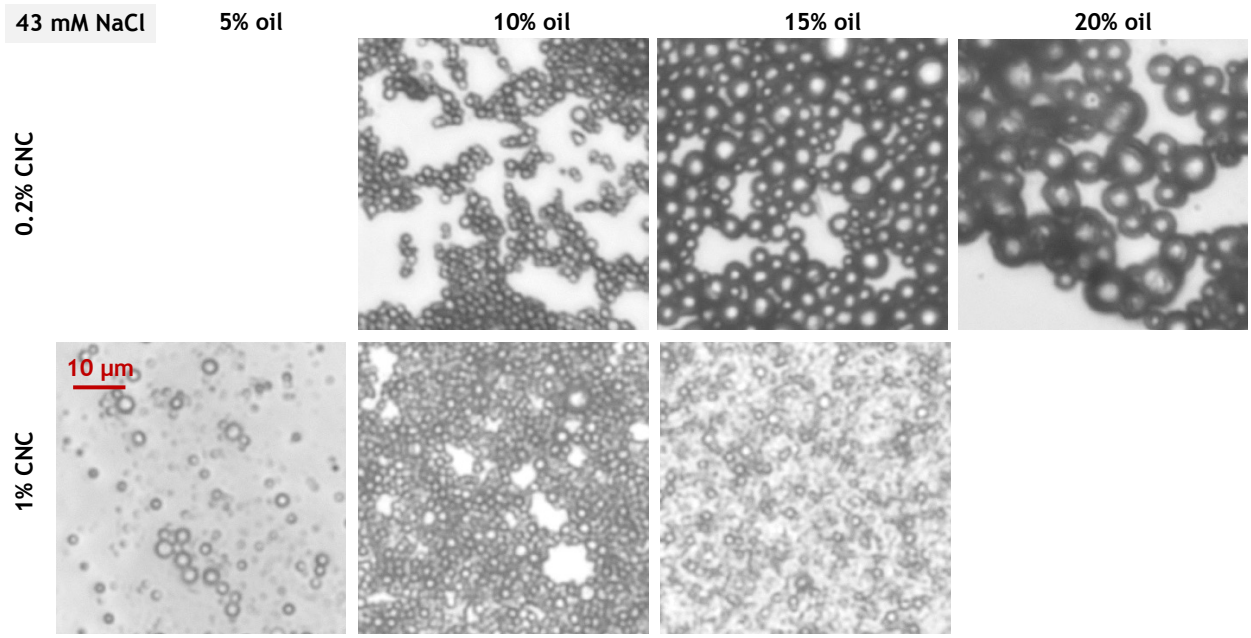


Figure 17. Optical microscopy images of CNC-coated wax microparticles (salt formulation, varying CNC concentration and oil fraction)

The optical microscopy images (Figure 17) at 43 mM NaCl show CNC-coated wax microparticles with clear variations in particle size distribution and spatial organization across formulations. While spherical particles are consistently observed, some conditions exhibit more clustering and chain-like aggregates with visible voids, whereas others display a more uniformly dispersed population of smaller droplets. Overall, the images indicate that 43 mM NaCl represents a transitional regime in which modest changes in oil fraction lead to noticeable differences in microparticle uniformity and aggregation behavior.

From a formulation perspective, these findings suggest an optimal oil fraction window between 10% and 15%, provided that the CNC-to-oil ratio remains constant. Within this range, emulsions achieve small, stable droplets with tunable rheology.

3.4 CNC and ODA formulation

In addition to the salt formulation discussed above, another approach to promote the CNC adsorption to wax microparticle is adding small amount of surfactant in the emulsion formulation. Octadecylamine (ODA) is selected as the surfactant. ODA is a long-chain aliphatic amine ($C_{18}H_{37}NH_2$) with a single primary amine group at one end and a hydrophobic hydrocarbon tail. In aqueous solution, ODA exhibits pH-dependent behavior. It has a pKa of ~10.6. Under acidic conditions, the amine group is protonated, forming a positively charged ammonium group ($–NH_3^+$),

and allowing it to adsorb to pristine CNC via the electrostatic interaction with the negatively charged sulfate ester groups ($–OSO_3^-$).

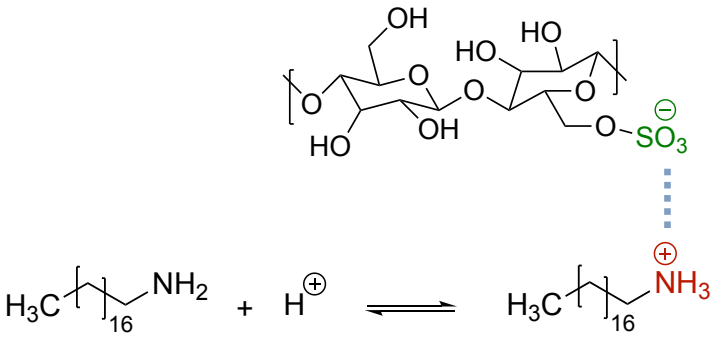


Figure 18. electrostatic interaction between sulfate ester group on CNC and protonated amine group of ODA.

3.4.1 Electrostatic and hydrophobic adsorption of ODA on CNC

The interaction CNC and ODA under acidic conditions in the absence of any coupling reagent is studied. The CNC dispersion was maintained at 1 wt%, while the ODA amount was varied to investigate its influence on surface modification and dispersion behavior.

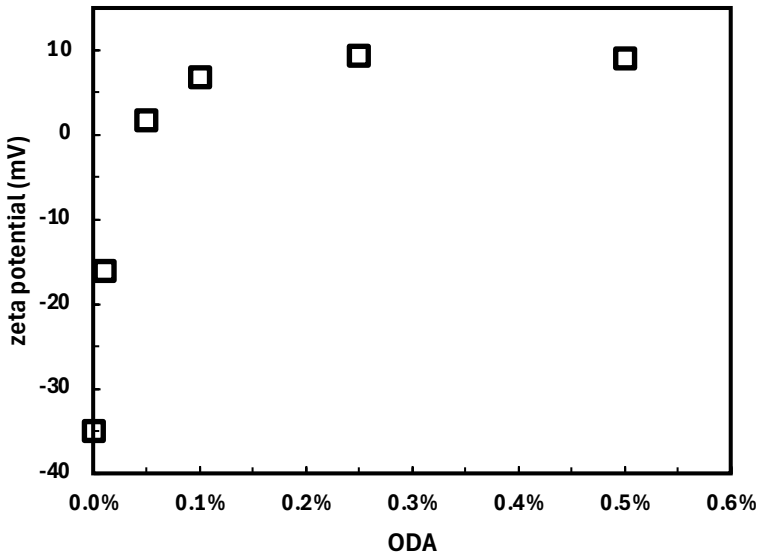


Figure 19. zeta potential measurements of 1 wt% CNC dispersed in different ODA solution of pH =3 (left to right: 0, 0.05, 0.1, 0.25, and 0.5 wt% ODA)

The zeta potential profile shows a clear transition from negative to positive values as ODA concentration increases, reflecting progressive adsorption of protonated amine groups onto the negatively charged CNC surface. At low ODA levels, the surface remains dominated by sulfate

groups. With increasing ODA, electrostatic attraction drives adsorption of $ODAH^+$, neutralizing surface charge and reducing the magnitude of the potential until charge reversal occurs around 0.03–0.05 wt%, where surface coverage approaches saturation. Beyond this point, the zeta potential plateaus near +10 mV, indicating complete or near-complete cationic layer formation and limited additional adsorption.

3.4.2 ODA concentration in emulsion

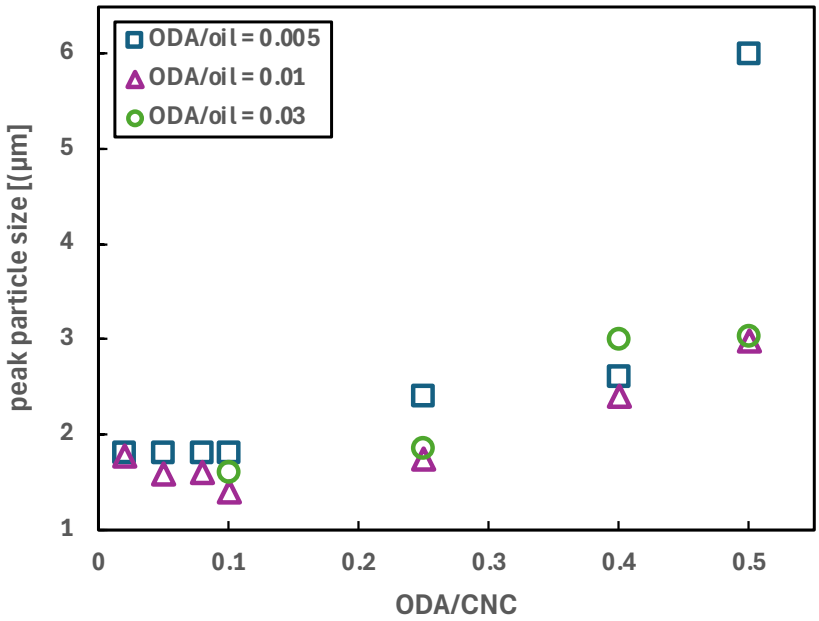


Figure 20. peak particle size measurements of CNC-coated wax microparticle suspensions (10% oil fractions, varying ODA/oil and ODA/CNC ratio)

Figure 17 presents the peak particle size as a function of the ODA-to-CNC mass ratio for three different ODA-to-oil ratios (0.005, 0.01, and 0.03). There is a distinct relationship between the degree of ODA addition and the resulting microparticle size, demonstrating how ODA mediates CNC adsorption at the oil–water interface and thereby controls the structural integrity of the emulsion droplets prior to wax solidification.

CNC is inherently hydrophilic and do not strongly adsorb at hydrophobic oil–water interfaces. The inclusion of ODA in acidic aqueous condition can improve CNC adsorption onto the wax droplets. The hydrophobic alkyl chains of ODA orient toward the oil phase, thereby rendering the CNC surface partially amphiphilic. However, excessive ODA addition can induce aggregation or interfacial destabilization by neutralizing CNC surface charge. Thus, the balance

between ODA and CNC determines the efficiency of interfacial coverage and the resulting particle size.

At low ODA-to-CNC ratios (≤0.1), the average particle size remains small, approximately 1.5–2 μm across all ODA/oil ratios. This size range corresponds to efficient droplet breakup and stabilization during emulsification. The limited addition of ODA provides sufficient surface hydrophobicity for CNCs to adsorb effectively at the oil–water interface without compromising their dispersion stability in the aqueous phase. The electrostatic repulsion between CNCs remains strong enough to prevent aggregation, ensuring uniform adsorption and stable droplet formation. In this regime, the CNCs act as efficient interfacial stabilizers, forming thin, rigid shells around the droplets that resist coalescence during emulsification and cooling.

As the ODA-to-CNC ratio increases beyond 0.1, the peak particle size begins to increase gradually, particularly for systems with lower ODA/oil ratios (0.005 and 0.01). This trend indicates that excess ODA begins to partially neutralize CNC surface charge, leading to reduced electrostatic stabilization and mild aggregation in the dispersion. When CNCs are less well-dispersed, their interfacial adsorption efficiency decreases, and droplet coalescence becomes more likely during emulsification. The resulting microparticles are larger, reflecting partial coalescence of droplets prior to wax solidification. Additionally, ODA molecules not bound to CNCs may accumulate at the interface, forming mixed surfactant layers that are less rigid and less resistant to droplet coalescence than CNC particle shells.

At high ODA-to-CNC ratios (≥0.4), the increase in particle size becomes more pronounced, particularly for the lowest ODA/oil ratio system (0.005), where the peak size exceeds 5 μm. This behavior arises from over-screening and aggregation effects. As more ODA is added, CNCs become heavily coated with hydrophobic alkyl chains, significantly reducing their colloidal stability. The resulting hydrophobized CNCs tend to form clusters rather than discrete nanoparticles. These clusters adsorb at the oil–water interface in irregular arrangements, leading to non-uniform interfacial coverage. The resulting emulsions are less stable, and droplet coalescence or flocculation occurs during emulsification. The larger particle size observed under these conditions thus reflects poor interfacial stabilization caused by excessive hydrophobization and charge neutralization.

In addition, the impact of ODA concentration in the formulation is studied by comparing the particle size trend of the three different ODA/oil ratios. With the oil fraction kept at 10%, at the lowest ODA/oil ratio (0.005), particle size increases sharply at high ODA/CNC ratios, indicating that when the total ODA concentration is low, small variations in ODA-to-CNC proportion

critically affect the charge balance and interfacial behavior. In contrast, at the highest ODA/oil ratio (0.03), particle sizes remain relatively small (<3 μm) even at higher ODA/CNC ratios. This suggests that at elevated ODA concentrations, sufficient free ODA is present to stabilize the oil–water interface directly, supplementing the CNC layer and preventing extensive coalescence.

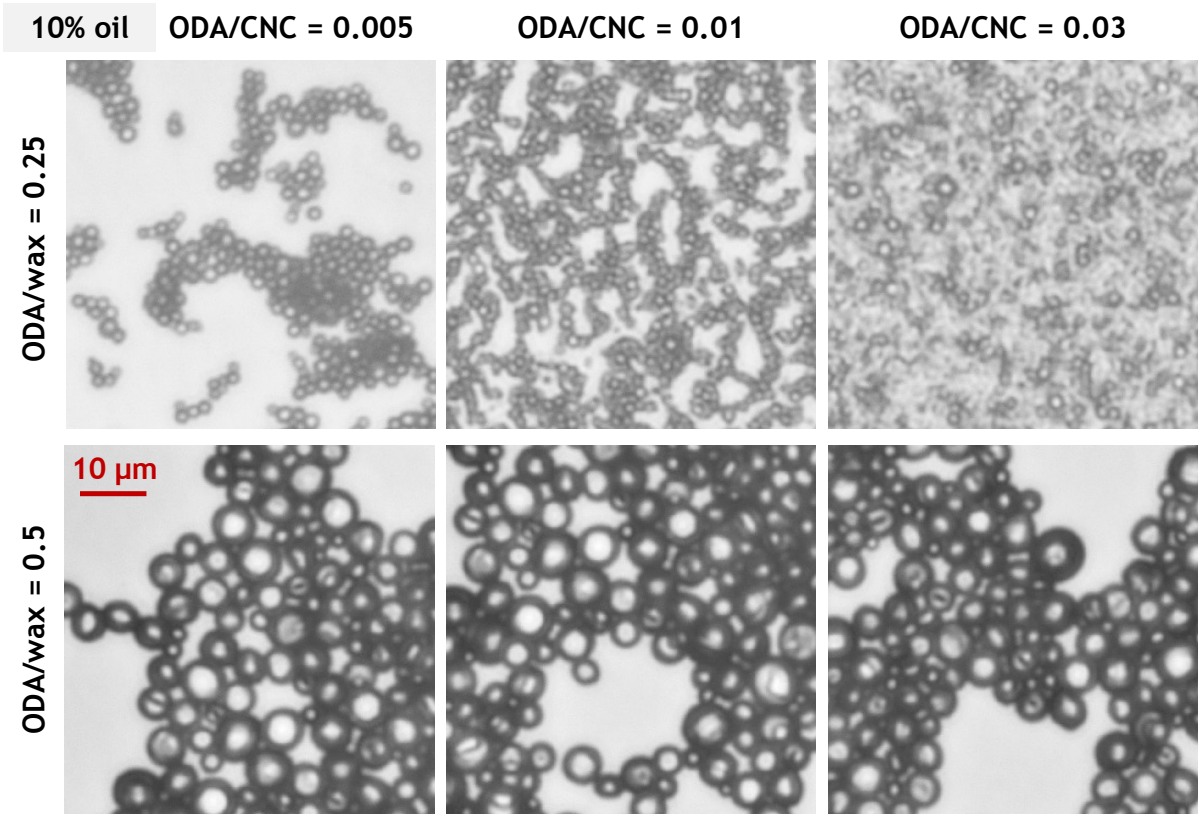


Figure 21. Optical microscopy images of CNC-coated wax microparticles (surfactant formulation)

The optical microscopy images (Figure 21) at 10% oil fraction reveal that the addition of ODA leads to the formation of clearly defined and closely packed wax microparticles, with noticeably improved particle circularity compared to salt formulations. While some clustering and interconnected structures remain visible at the optical scale, the droplets are more uniform in size and less prone to irregular aggregation. This trend is corroborated by the SEM images (Figure 22), which show predominantly spherical, well-defined microparticles with smoother surfaces. At lower ODA/oil ratios, larger particles with occasional surface imperfections are observed, whereas increasing the ODA/oil ratio produces a denser population of smaller, more uniformly sized microparticles. Together, the optical and SEM results indicate that ODA modification improves

CNC amphiphilicity and interfacial stabilization, suppressing droplet coalescence during emulsification and yielding more uniform wax microparticles upon solidification.

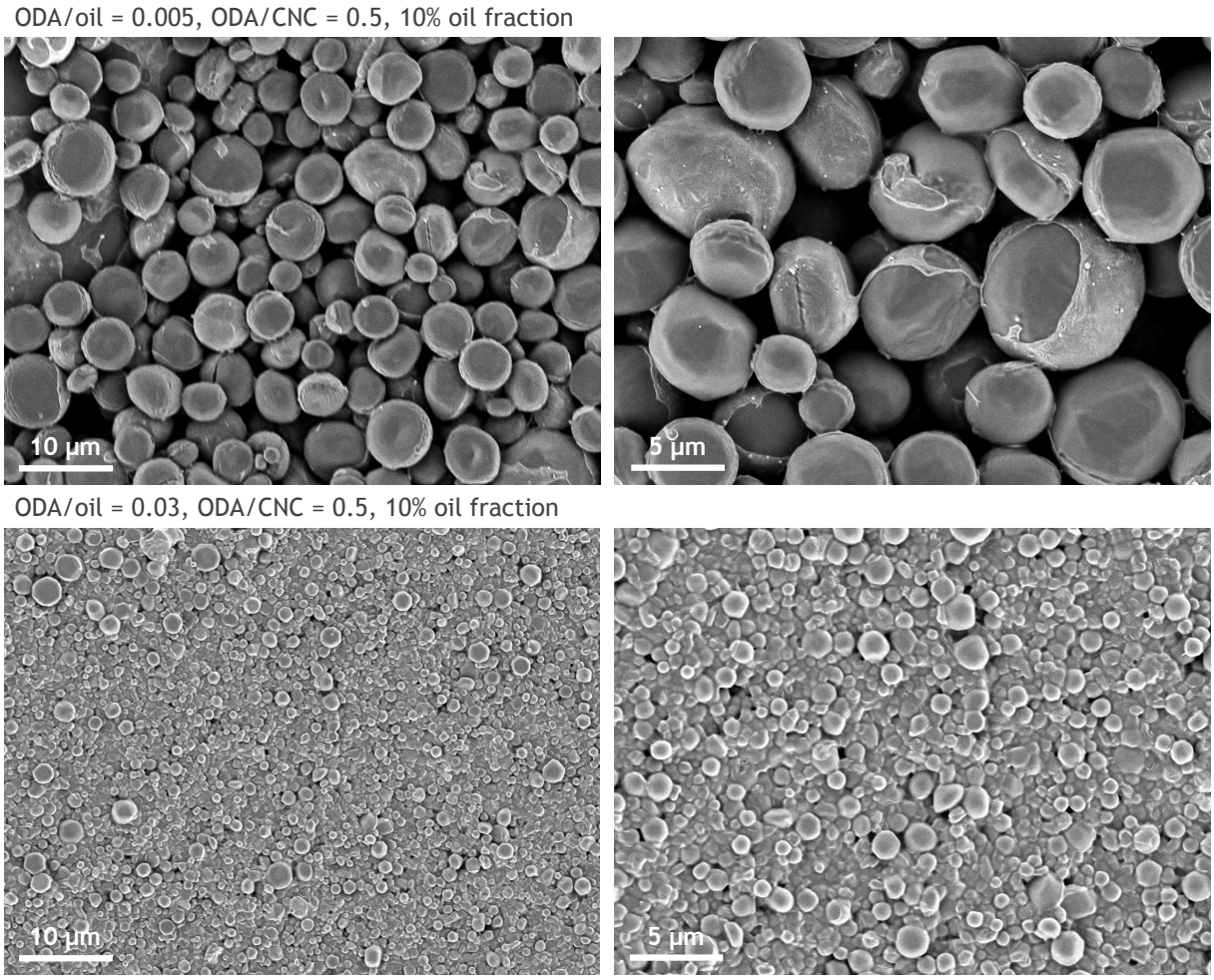


Figure 22. SEM images of CNC-coated wax microparticles (surfactant formulation)

Overall, the results indicate that there exists an optimal ODA/CNC ratio that maximizes interfacial stabilization efficiency. At low ratios, CNCs are too hydrophilic to fully adsorb; at moderate ratios (≈0.05–0.1), CNCs acquire partial amphiphilicity and adsorb effectively; and at high ratios, aggregation and charge neutralization reduce stability. The dependence of droplet size on ODA concentration therefore reflects a balance between surface modification (hydrophilicity to hydrophobicity transition) and colloidal stability (repulsion to aggregation).

The consistent minimum particle size near an ODA/CNC ratio of 0.05–0.1 for all ODA/oil conditions suggests that this ratio provides the ideal hydrophilic–hydrophobic balance for interfacial anchoring without destabilization. The presence of ODA therefore acts as a molecular bridge

between CNCs and the oil phase, controlling their amphiphilicity and ultimately the morphology of the final wax microparticles.

3.5 Conclusions

This chapter contains investigation into the formulation, stabilization mechanisms, and structural transitions of paraffin wax Pickering emulsions and their corresponding solid wax suspensions stabilized by CNC. The work focused on understanding how interfacial and colloidal interactions, modulated by electrolyte screening and surfactant-assisted adsorption, govern the formation, stability, and microstructure of CNC-based emulsion systems. Two primary formulation strategies were examined: one relying solely on salt-screened CNC dispersions, and the other employing ODA as an auxiliary surfactant to enhance CNC adsorption at the oil–water interface.

Overall, the results presented in this chapter establish a comprehensive understanding of how CNCs stabilize paraffin wax emulsions through physical adsorption, interparticle interactions, and surface modification. Ionic strength dictates the balance between electrostatic repulsion and adsorption energy; CNC concentration defines interfacial completeness and bulk rheology; oil fraction governs the geometric demand for stabilizer coverage; and ODA provides a tunable means to bridge the hydrophilic CNC surface and hydrophobic wax phase. Together, these parameters form an interconnected formulation framework that determines droplet size, stability, suspension texture, and surface wettability.

In conclusion, CNC-stabilized paraffin wax Pickering emulsions represent a versatile and sustainable platform for designing solid–liquid dispersions with controllable microstructure and surface properties. Through careful optimization of ionic strength, CNC loading, oil fraction, and ODA concentration, it is possible to achieve precise control over interfacial architecture and phase behavior, enabling the production of wax microparticles and coatings with tailored hydrophilicity, mechanical stability, and morphology. The insights gained here provide a fundamental basis for future development of CNC-based colloidal systems for applications in coatings, encapsulation, and phase-change materials.

Chapter 4 Wax Microparticle Coatings: Performance Comparison between Fog and Dew Water Harvesting

4.1 Introduction

This chapter focuses on using the CNC-wax particle as a surface coating and evaluating its performance for fog and dew water harvesting. While the previous chapter investigated the influence of formulation parameters on emulsion particles, the next step is to determine how these structural and surface features translate into practical performance under both water droplet deposition and vapor water condensation processes. These two pathways represent distinct yet complementary strategies for harnessing atmospheric moisture.

As reviewed in Chapter 2, natural organisms, such as desert beetles and spider webs, have inspired the design of engineered surfaces that enhance the capture and transport of water. For AWH devices, their efficiency can be enhanced by controlling surface chemistry and morphology to promote droplet nucleation, directional water transport, and droplet shedding. An optimized surface can increase the fog and dew water collection performance by balancing hydrophilic regions for nucleation and hydrophobic domains for droplet removal, or by incorporating hierarchical roughness to accelerate droplet growth and departure.

A key gap in the literature is the lack of side-by-side comparisons of fog and dew water collection on identical materials. Compounding this, the field is limited by the prevalent use of fluorinated coatings and lithography, which pose major challenges for scalable and environmentally compatible production. Therefore, the objective of this chapter is to systematically compare the water collection performance of scalable and low-cost alternative CNC-wax microparticle coatings under fog and dew conditions. In this chapter, we will focus on the following: (i) investigation of the correlation between Pickering emulsion particle properties and wettability, morphology, and overall harvesting performance of the coated substrate; and (ii) observation of the droplet growth and drainage behaviors during fog exposure and dew formation.

4.2 Experimental

4.2.1 Surface fabrication procedure

Substrate cleaning

Glass microscope slide and 5052 aluminum sheet (20 GA) were used as test substrates. The substrates were washed with acetone, iso-propanol, 0.01 M HCl, rinsed with Milli-Q water, and dried with clean air.

Spraying

The CNC-wax particle suspension prepared in 3.2.2 was sprayed onto the substrate using a spray gun (Figure 18). The spraying content was heated using a heat gun to improve water evaporation and wax particle adhesion onto the substrate surface. The sprayed samples were allowed to dry for 1 day in the fume hood prior to further testing.

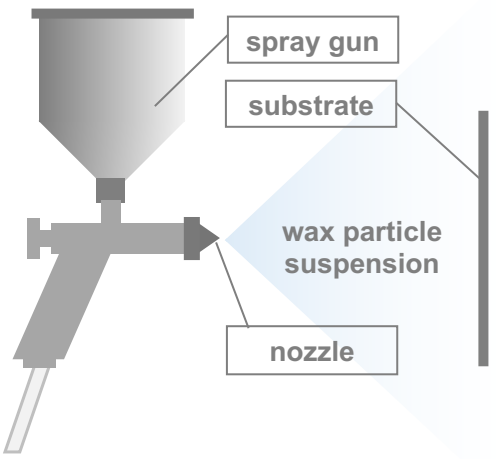


Figure 23. Spray coating procedure

4.2.2 Surface characterization

Contact angle

The static contact angle was measured using the sessile drop method on a tensiometer DCAT 11(Dataphysics). A 5 μL water droplet was dispensed onto the test surface using an auto-dosing system equipped with a 500 μL syringe needle. Once the droplet approached an equilibrium condition, a side-view image was captured using a digital camera. The static contact angle was then determined by analyzing the captured image with ImageJ software for precise analysis.

Contact angle hysteresis

Advancing and receding contact angles were measured using the sessile-drop goniometry. A droplet was first placed on the test surface, and its volume was increased from 3 μL to 10 μL to determine the advancing contact angle from the expanding contact line. Subsequently, the droplet volume was decreased back to 3 μL to obtain the receding contact angle from the contracting contact line.

4.2.3 Fog water harvesting tests

Fog water harvesting tests were conducted following the set up in Figure 19. The fog stream was directed horizontally toward the test surface mounted at the center opening on top of a balance. The droplet deposited on the test surface were allowed to slide off and be collected by the balance. Fog flow (300 mL/hr) and humidity (RH = 80 %) were stabilized before each run. Tests were conducted at a fixed surface to fog flow distance (≈10 cm) for up to 1 hr fog exposure.

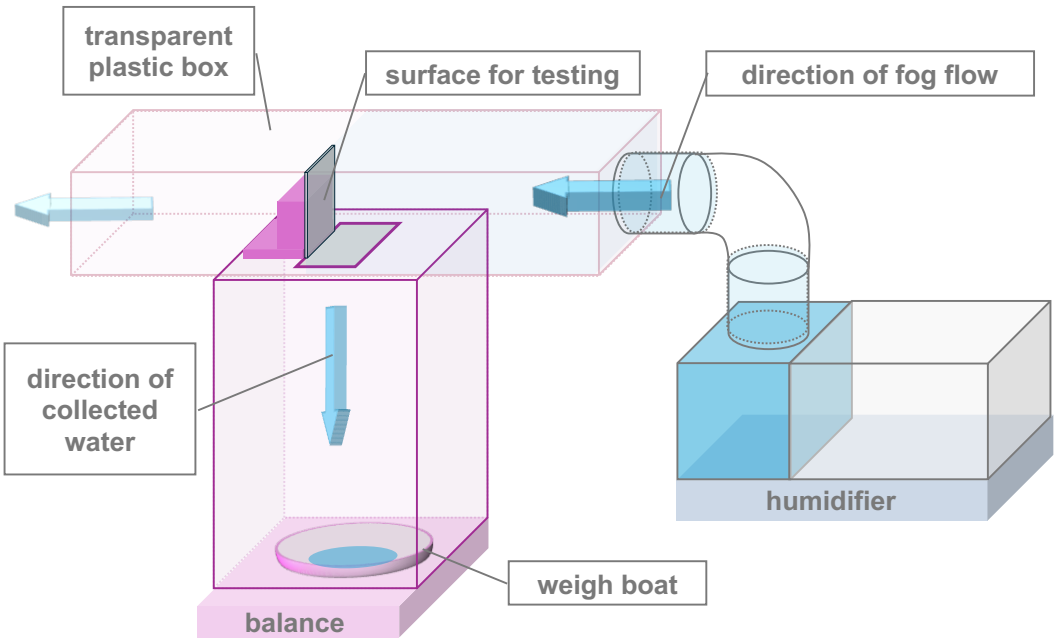


Figure 24. fog harvesting test set up

4.2.4 Humid air condensation test

Condensation performance was measured using a Peltier-based setup in Figure 20. The test surface was mounted on the cold side of a temperature-controlled Peltier module, with surface temperature maintained below dew point a controlled subcooling (ΔT = 5 °C). Tests were conducted in lab ambient conditions for up to 45 min of surface cooling.

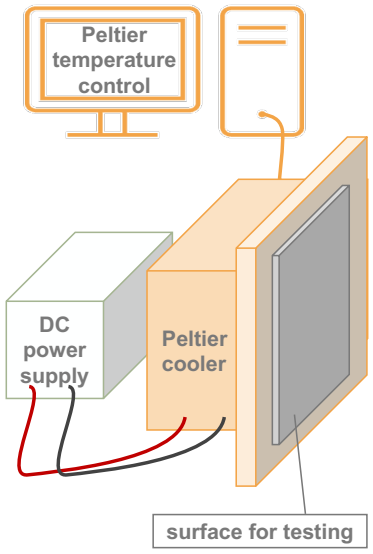


Figure 25. condensation test set up

4.3 Static and dynamic contact angle

This section examines how the Pickering emulsion formulation translates into measurable wetting behavior on the coated surfaces. Static and dynamic contact angles serve as complementary indicators of surface chemistry, texture, and droplet mobility. The static angle reflects the equilibrium balance of surface energies, while the advancing, receding, and hysteresis angles reveal whether the surface sustains a Cassie state or exhibits Wenzel-like pinning. As established in the previous formulation analysis, parameters such as CNC concentration and ionic strength control the interfacial organization during emulsification; these microscopic arrangements are now expressed macroscopically through differences in apparent contact angle and hysteresis. Together, these measurements provide a direct link between emulsion design and surface wetting properties.

4.3.1 Static contact angle

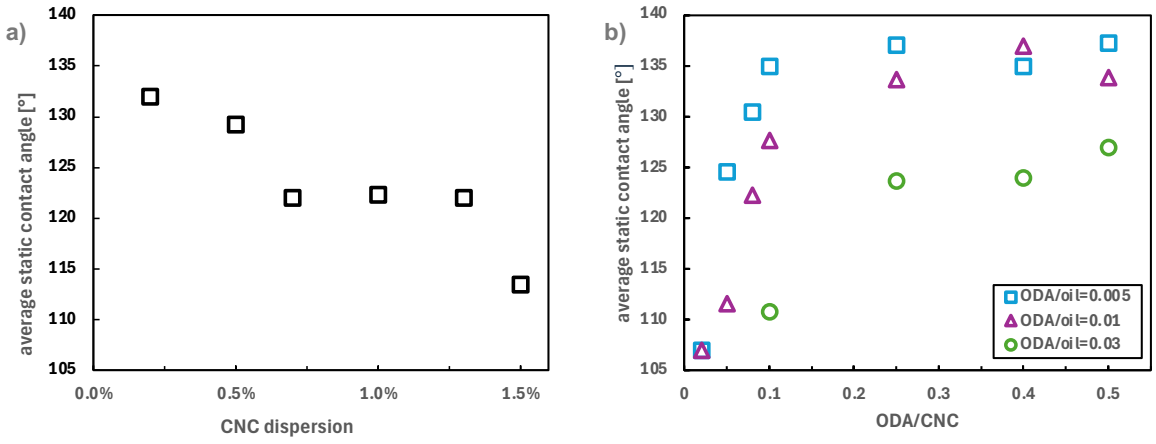


Figure 26. average static contact angle measurements of coated surfaces. Synthesis formulation: a) 43 mM NaCl, 10% oil fraction, varying CNC; b) 10% oil fraction, varying ODA and CNC.

Salt formulation coating

Figure 21a presents the average static contact angle as a function of CNC dispersion concentration, showing a marked transition from hydrophobic to hydrophilic behavior as CNC content increases.

At low CNC concentrations (below 0.5 wt%), the measured contact angles were between 125° and 135°, indicating a highly hydrophobic surface dominated by exposed wax domains. In this region, CNC coverage of the wax particles is incomplete, forming discrete hydrophilic patches surrounded by continuous hydrophobic wax regions. The limited surface fraction of CNCs is insufficient to significantly alter the overall surface energy, and the water droplet rests primarily on the wax phase, similar to pure paraffin-like materials. The strong hydrophobic character suggests that the CNCs are sparsely distributed, with minimal overlap or network formation at the particle surface.

As CNC concentration increases to 0.6 to 1 wt%, a gradual reduction in the contact angle is observed, reaching approximately 115° at 1 wt%. This change reflects the increased surface presence of CNCs, which introduce hydrophilic hydroxyl and sulfate groups to the outer surface. Under these conditions, the surface becomes more heterogeneous at the nanometer length scale, exhibiting both hydrophobic wax and hydrophilic CNC domains. The water droplets interact with the composite surface, and its apparent contact angle is governed by the area-weighted contribution of both components. This behavior aligns with the Cassie–Baxter wetting model, where the apparent contact angle depends on the fractional coverage of each surface type. The moderate reduction in contact angle in this concentration range corresponds to partial CNC percolation across the wax surface but not yet to full hydrophilic coverage.

At CNC concentrations above 1 wt%, a further decrease in the contact angle occurs, suggesting the transition from a wax-dominated to a CNC-dominated surface. The water droplet now primarily contacts the CNC-rich regions, and spreading is favored due to hydrogen bonding between water and surface hydroxyl groups. The hydrophilic nature of CNCs, enhanced by the presence of sulfate groups introduced during acid hydrolysis, contributes to a high surface energy and strong affinity for water. As a result, the coating behaves as a hydrophilic surface, and the droplet rapidly flattens, producing a low apparent contact angle.

The correlation between CNC concentration and static contact angle demonstrates that the wettability of CNC–wax coatings can be tuned over a wide range without chemical modification. By simply adjusting CNC loading during emulsification, the resulting coatings can transition from water-repellent to highly hydrophilic. Low CNC loadings produce smooth, wax-dominated hydrophobic coatings, whereas high CNC loadings create rough, hydrophilic surfaces rich in hydroxyl groups. Intermediate loadings yield partially hydrophilic coatings with mixed surface chemistry, offering a balance between water resistance and surface adhesion.

Surfactant formulation coating

Figure 21b. Illustrates the effect of ratio of ODA to CNC on the static contact angle. At low ODA/CNC ratios (<0.1), the contact angles remain around 105–120°, indicating that the CNC-coated paraffin surfaces are only partially hydrophobized due to limited ODA adsorption. As the ODA/CNC ratio increases, the CA rises sharply, reaching 130–138° at ODA/CNC ≈ 0.25–0.5 for ODA/oil ratios of 0.005 and 0.01. This increase suggests enhanced ODA adsorption onto CNC surfaces, which reduces surface polarity and improves compatibility with the oil phase. The plateau observed beyond an ODA/CNC ratio of 0.25 suggesting near-saturation of ODA at the CNC interface, which is consistent with a Langmuir-type adsorption behavior where additional surfactant contributes little to further hydrophobization.

Comparing across the ODA/oil ratios, the samples with the lowest ODA/oil (0.005) exhibit the highest CAs at saturation, reflecting more efficient surface modification per unit of ODA, possibly due to lower competition for interfacial adsorption sites. In contrast, increasing ODA/oil to 0.03 leads to consistently lower CAs (110–125°), indicating that excess ODA in the continuous phase may cause partial desorption or micelle formation, limiting its interfacial effectiveness. Overall, the data show that static contact angle correlates positively with the ODA/CNC ratio up to a saturation point but inversely with the ODA/oil ratio beyond the optimal loading, highlighting a balance between ODA availability and interfacial organization in controlling CNC-mediated surface hydrophobicity.

4.3.2 Contact angle hysteresis

Contact angle hysteresis of surfactant formulation coating was measured to further characterize the droplet dynamics on the surface. The CAH values, ranging from 25° to 59°, exhibit less sensitivity to formulation changes than static CA. At low ODA/oil ratios (0.005), CAH increases with ODA/CNC, consistent with partial ODA adsorption and heterogeneous interfacial

coverage leading to pinning effects. As ODA/oil increases to 0.03, CAH decreases substantially (to ~25–36°), indicating more uniform ODA–CNC interfacial assembly and reduced surface heterogeneity. This inverse relationship between CAH and ODA/oil ratio suggests that excess ODA leads to a smaller hysteresis with enhanced dynamic wetting uniformity. Collectively, the data imply that while overall hydrophobicity (CA) saturates at moderate ODA/CNC ratios, the uniformity and stability of the coating (CAH) continue to improve with increased ODA availability. This highlights the importance of balancing ODA concentration relative to CNC to achieve optimal interfacial control in Pickering emulsion-derived microparticles.

4.3.3 Selection of coating for water harvesting

Four representative samples—A (ODA/CNC = 0.1, ODA/oil = 0.03), B (ODA/CNC = 0.02, ODA/oil = 0.01), C (ODA/CNC = 0.1, ODA/oil = 0.01), and D (ODA/CNC = 0.5, ODA/oil = 0.005)—were selected from the contact angle (CA) and contact angle hysteresis (CAH) plot (Figure 22) to evaluate the water harvesting performance under different surface wetting regimes. These conditions were selected to represent the distinct combinations of macroscopic hydrophobicity and droplet mobility, which together govern condensation nucleation and droplet drainage behavior.

Samples A and B exhibit relatively moderate static contact angles (110–120°) but differ significantly in CAH, indicating surfaces with comparable wettability yet different droplet pinning characteristics. Sample A, with lower CAH, represents a surface where droplets are more mobile, potentially favoring faster coalescence and drainage. Sample B, having higher hysteresis, corresponds to stronger droplet adhesion, expected to enhance initial nucleation but reduce droplet mobility. Sample C, with a high CA (~135°) and low CAH (~30°), exemplifies a highly hydrophobic yet slippery surface ideal for rapid droplet shedding, thereby maximizing water collection efficiency through frequent renewal of nucleation sites. Conversely, sample D combines high CA and high CAH, representing a sticky superhydrophobic state where droplets form easily but exhibit strong adhesion, leading to slower drainage and possible coalescence-induced losses.

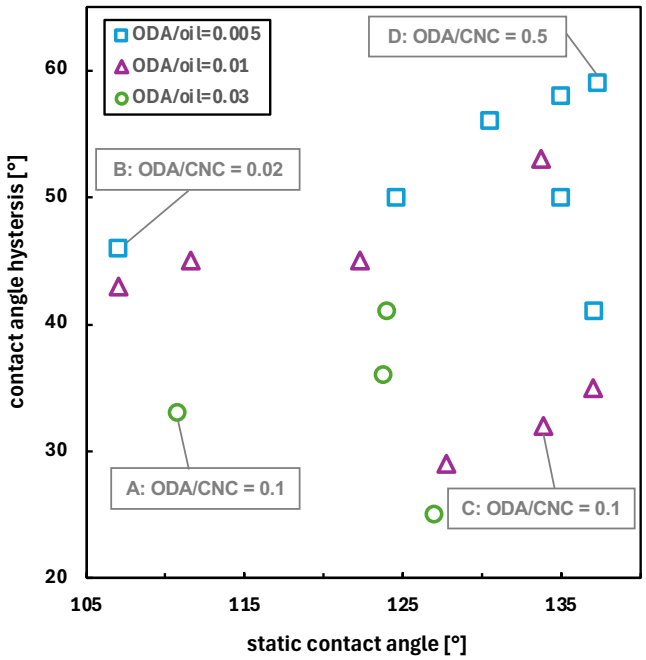


Figure 27. Static contact angle vs. contact angle hysteresis of coated surfaces. Synthesis formulation: 10% oil fraction, varying ODA and CNC.

4.4 Fog water harvesting results

The fog collection efficiency of four surfaces was evaluated over a 60-minute period of continuous fog exposure. Samples A to D represent the four distinct wettability regimes described in Section 4.3.3. Figure 23 plots the amount of water collection over fog exposure time. Approximately after 20 minutes of exposure, all four surfaces have the first droplet sliding off by gravity. With further exposure time, the drainage and coalescence of water become slightly different for each surface. Surface C (high CA, low CAH) has the greatest cumulative water collection, indicating that hydrophobic yet mobile surfaces favor both efficient droplet capture and rapid removal, as the low hysteresis enables frequent droplet shedding and continual surface renewal for subsequent impingement. Surface A (low CA, low CAH) also demonstrated high collection efficiency. Its more wettable, moderately hydrophobic character enhances droplet spreading and coalescence, while its low hysteresis promotes filmwise drainage.

In contrast, Surface D (high CA, high CAH) exhibited intermediate performance. Although its high contact angle supports initial droplet adhesion, the large hysteresis causes droplets to become strongly pinned, resulting in delayed coalescence and intermittent detachment events. This limits the continuous renewal of active collection sites and thus reduces the overall water flux. The

poorest performance was recorded for Surface B (low CA, high CAH). The combination of strong wetting and high hysteresis led to the formation of a stable, pinned water film that hindered both new droplet impingement and gravity-driven drainage.

Surfaces A and C, both exhibiting low CAH values (below approximately 25°), outperformed the high-hysteresis surfaces B and D, confirming that CAH plays the dominant role in controlling fog water removal. Low hysteresis minimizes droplet pinning, facilitates coalescence, and promotes efficient gravitational shedding, thereby maintaining exposed regions for continued fog capture. The static contact angle exerts a secondary but still significant influence. When comparing surfaces with similar CAH, the surface with higher CA (Surface C) consistently yields higher water collection than the one with lower CA (Surface A), reflecting the improved fog droplet capture efficiency of hydrophobic microtextures. Hydrophobic surfaces can better retain airborne microdroplets upon impact, allowing them to coalesce before being shed. However, this benefit disappears when hysteresis is high, as observed in surfaces B and D, where droplet pinning prevents timely removal.

Overall, the results support the capture–release balance model of fog harvesting efficiency. The most efficient collection occurs when sufficient adhesion is present to retain impinging fog droplets, yet hysteresis is low enough to allow their rapid coalescence and detachment once a critical size is reached. In summary, surfaces with low hysteresis consistently achieve greater fog water yield, and coatings with moderately to highly hydrophobic contact angles (approximately 130–135°) and low CAH values (below 20°) represent the most effective configuration for fog water harvesting under the present experimental conditions.

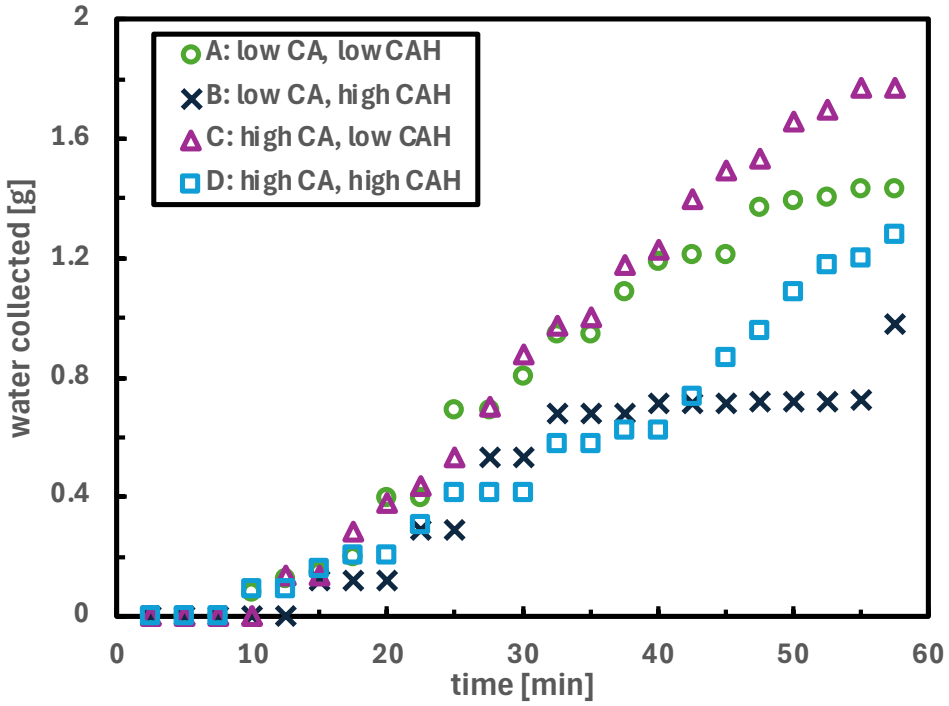


Figure 28. collected water vs. fog exposure time

4.5 Condensation results

The humid air condensation efficiency of four surfaces was evaluated over a 45-minute period of continuous surface cooling. Samples A to D represent the four distinct wettability regimes described in Section 4.3.3. Figure 24 describes the amount of liquid water collection over cooling exposure time. The overall condensation behavior differs substantially from the fog collection trends discussed earlier, reflecting the contrasting physical mechanisms of vapor-phase condensation and liquid droplet deposition on surfaces.

For the first 25 minutes, tiny condensed droplets remain adhered to the surface; therefore, no water collection occurs on all surfaces. After this nucleation and early droplet growth period, the collection rates diverge as the condensed droplets coalesce and reach the critical size for drainage by gravity. Surface A (low CA, low CAH) displays the highest cumulative water collection. Its strong wettability facilitates high nucleation density, promoting rapid condensation. The low hysteresis further enables smooth drainage of the resulting condensate film. Surface C (high CA, low CAH) also exhibits a similar final yield. Although its hydrophobic nature slightly reduces nucleation density compared to Surface A, the low hysteresis allows frequent droplet detachment. Similarly, Surfaces with high hysteresis (B and D) exhibit reduced condensation. The retained droplets merge into

larger, immobile patches, creating a quasi-filmwise regime that limits the overall condensation rate. The results highlight the role of water drainage efficiency in condensation-driven water harvesting. While a low CA promotes abundant nucleation by lowering the energy barrier for droplet formation, high hysteresis negates this benefit by trapping condensate on the surface.

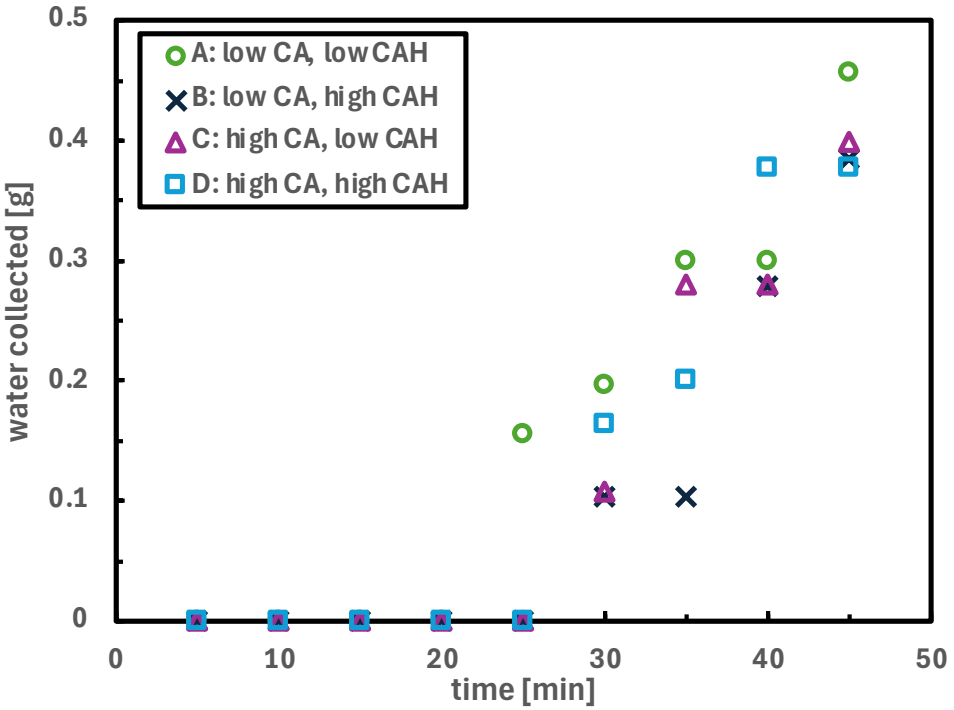


Figure 29. collected water vs. surface cooling time

4.6 Conclusions

This chapter describes how the structure of CNC–coated wax microparticles directly governs the macroscopic wetting behavior of the resulting coated surfaces and, consequently, their water-harvesting performance. Systematic variation of the ODA/CNC and ODA/oil ratios revealed that both the static contact angle (CA) and contact angle hysteresis (CAH) are strongly dependent on the balance between surfactant adsorption and CNC interfacial packing. Increasing the ODA/CNC ratio enhanced hydrophobicity up to a saturation point, reflected by CA values approaching 135–140°, while further ODA addition or excessive oil content led to reduced interfacial organization and increased surface heterogeneity, manifested as higher CAH. In contrast, surfaces prepared from emulsions with optimized ODA/CNC ratios exhibited low hysteresis and stable high contact angles, characteristic of well-ordered hydrophobic coatings.

Comparative water-harvesting experiments under fog and dew conditions revealed distinct functional dependencies on surface wetting state. Fog harvesting favored surfaces with moderate to high hydrophobicity and low CAH, where sufficient initial droplet capture was combined with minimal pinning, enabling efficient coalescence and frequent shedding. Dew collection, however, was enhanced on more mobile surfaces exhibiting lower CAH, where reduced pinning facilitated rapid droplet shedding and surface renewal. Together, these findings confirm that tuning emulsion formulation allows precise control over CNC–ODA surface architecture, enabling the design of hybrid coatings optimized for both fog and dew water collection.

Chapter 5 Conclusions

5.1 Conclusions

This thesis describes the design, synthesis, and performance evaluation of sustainable, cellulose nanocrystal (CNC) and paraffin wax-based coatings fabricated via Pickering emulsion. The work established a scalable and sustainable route for fabricating textured surfaces capable of manipulating wetting behavior and collecting atmospheric water from dew and fog. By systematically varying the formulation parameters—ionic strength, CNC concentration, oil fraction, and surfactant content—the interfacial assembly of CNCs at the oil–water boundary and the resulting particle morphology were effectively tuned to control coating hydrophobicity and droplet mobility.

In Chapter 3, the effects of NaCl concentration and CNC concentration on emulsion stabilization and particle size were quantified. Increasing ionic strength screened electrostatic repulsion between CNCs, promoting their adsorption at the oil–water interface and leading to smaller, more uniform wax particles up to an optimal salt concentration. Similarly, a moderate CNC loading enhanced emulsion stability and yielded particles with rough, hierarchical surfaces. Incorporation of ODA further modified the CNC surface charge, improving compatibility with the oil phase and enabling dense particle coverage. The combined effect of these parameters established a formulation map linking emulsion stability and microparticle size distribution to interfacial charge and surfactant chemistry.

In Chapter 4, coatings prepared from these microparticle suspensions were characterized by static and dynamic water contact angles. The static angle reflected the composite chemistry and micro texture following the Cassie–Baxter model, while the contact angle hysteresis (CAH) captured droplet pinning and mobility. Formulations with moderate salt screening and optimized CNC/ODA balance achieved high static contact angles ($> 130°$) and low CAH ($< 20°$). Comparative tests under controlled dew and fog conditions revealed that such surfaces maintained efficient droplet shedding and enhanced cumulative water collection. In dew condensation, surface wetting features governed nucleation and coalescence, whereas in fog collection, macro-scale droplet mobility and drainage dominated performance. Together, these results highlight the dual function of CNC-wax coatings as both hydrophobic and water-harvesting surfaces without relying on fluorinated chemistries.

Overall, the study demonstrates a robust, low-cost fabrication strategy that integrates renewable cellulose nanocrystals with paraffin wax to achieve tunable wettability and water collection efficiency. The approach bridges interfacial design principles with sustainable materials engineering, offering a path toward scalable, PFAS-free functional coatings for environmental and industrial applications.

5.2 Future work

While this study addressed key relationships between formulation parameters, interfacial assembly, and macroscopic performance, several open questions remain that define the path forward for continued exploration.

5.2.1. Remaining questions in Pickering emulsion design

The interfacial adsorption behavior of CNCs on wax droplets needs further quantitative analysis. Future work should employ in situ characterization methods such as interfacial rheology, cryo-TEM, or small-angle scattering to capture CNC packing density and orientation at the oil–water interface.

In addition, formulation with further changes in the oil phase composition or CNC modification should be studied. Tuning the intrinsic hydrophobicity of the oil phase (such as replacing it with more hydrophilic bio-based waxes), or ODA grafting on CNC, could have a further impact on the emulsion particle properties, leading to coating with enhanced mechanical stability, biodegradability, and wetting properties.

Lastly, developing predictive models that link surface charge, ionic strength, and droplet size distributions could provide a quantitative design tool for scaling up CNC-based emulsions.

5.2.2. Remaining questions in water harvesting mechanisms

In the context of atmospheric water capture, the observed differences between dew and fog collection highlight the need to decouple condensation kinetics, droplet coalescence dynamics, and drainage behavior. Future studies should integrate real-time optical imaging and thermal mapping to directly observe droplet nucleation and heat transfer on CNC-wax coatings. Quantifying how contact angle hysteresis evolves over repeated condensation cycles will help understand wetting degradation and transition from Cassie–Baxter to Wenzel states. Additionally, the role of non-condensable gases and ambient air flow—critical in real fog and humid-air conditions—should be

systematically varied to bridge laboratory and environmental performance. Exploring biphilic patterning or gradient coatings using controlled deposition of CNC-wax particles could enhance directional droplet transport and improve cumulative water yield.

5.2.3. Integration, durability, and applications

To scale this tunable coating system for commercial use, further studies on the mechanical durability, UV stability, and long-term water repellency of the coatings under cyclic wetting and drying should be pursued. Moreover, for broader applications such as anti-fogging, anti-icing, or thermal management, the CNC-wax coating could be further expanded into a functional hybrid system by the incorporation of photothermal or conductive additives.

References

[1] A. Agrawal and A. Kumar, "A comprehensive review of fresh water production from atmospheric air – techniques, challenges and opportunities," *Environ. Dev. Sustain.*, July 2024, doi: 10.1007/s10668-024-05211-2.

[2] W. Zeng, T. You, and W. Wu, "Passive atmospheric water harvesting: Materials, devices, and perspectives," *Nano Energy*, vol. 125, p. 109572, June 2024, doi: 10.1016/j.nanoen.2024.109572.

[3] K. Chen, Y. Tao, and W. Shi, "Recent Advances in Water Harvesting: A Review of Materials, Devices and Applications," *Sustainability*, vol. 14, no. 10, Art. no. 10, Jan. 2022, doi: 10.3390/su14106244.

[4] Martin, "Goal 6: Water and Sanitation," United Nations Sustainable Development. Accessed: Sept. 11, 2025. [Online]. Available: https://www.un.org/sustainabledevelopment/water-and-sanitation/

[5] *16 Principles and Applications of Atmospheric Water Harvesting*. Accessed: Apr. 22, 2025. [Online]. Available: https://learning.oreilly.com/library/view/handbook-of-water/9781119478959/c16.xhtml

[6] *17 Dew Harvesting on High Emissive Natural and Artificial Passive Surfaces*. Accessed: Apr. 22, 2025. [Online]. Available: https://learning.oreilly.com/library/view/handbook-of-water/9781119478959/c17.xhtml

[7] M. Dong, Z. Zhang, Y. Shi, X. Zhao, S. Fan, and Z. Chen, "Fundamental Limits of the Dew-Harvesting Technology," *NANOSCALE MICROSCALE Thermophys. Eng.*, vol. 24, no. 1, pp. 43–52, Jan. 2020, doi: 10.1080/15567265.2020.1722300.

[8] B. Tashtoush and A. Alshoubaki, "Atmospheric water harvesting: A review of techniques, performance, renewable energy solutions, and feasibility," *Energy*, vol. 280, p. 128186, Oct. 2023, doi: 10.1016/j.energy.2023.128186.

[9] Y. Zhong *et al.*, "Bridging materials innovations to sorption-based atmospheric water harvesting devices," *Nat. Rev. Mater.*, vol. 9, no. 10, pp. 681–698, Oct. 2024, doi: 10.1038/s41578-024-00665-2.

[10] D. Beysens, "Dew nucleation and growth," *Comptes Rendus Phys.*, vol. 7, no. 9–10, pp. 1082–1100, Nov. 2006, doi: 10.1016/j.crhy.2006.10.020.

[11] A. Lee, M.-W. Moon, H. Lim, W.-D. Kim, and H.-Y. Kim, "Water harvest via dewing," *LANGMUIR*, vol. 28, no. 27, pp. 10183–10191, July 2012, doi: 10.1021/la3013987.

[12] P. L. Singh and B. S. Sikarwar, "Condensation of Moist Air on Mesh-like Surfaces," *ASIAN J. WATER Environ. Pollut.*, vol. 17, no. 2, pp. 65–72, 2020, doi: 10.3233/AJW200022.

[13] C.-Y. Lin, T.-A. Teng, H.-K. Chang, and P.-Y. Chen, "Desert Beetle-Inspired Hybrid Wettability Surfaces for Fog Collection Fabricated by 3D Printing and Atmospheric Pressure Plasma Treatment," *Biomimetics*, vol. 10, no. 3, p. 143, Mar. 2025, doi: 10.3390/biomimetics10030143.

[14] A. R. Parker and C. R. Lawrence, "Water capture by a desert beetle," *Nature*, vol. 414, no. 6859, pp. 33–34, Nov. 2001, doi: 10.1038/35102108.

[15] J. Ju, H. Bai, Y. Zheng, T. Zhao, R. Fang, and L. Jiang, "A multi-structural and multi-functional integrated fog collection system in cactus," *Nat. Commun.*, vol. 3, no. 1, p. 1247, Dec. 2012, doi: 10.1038/ncomms2253.

[16] Z. Pan, W. G. Pitt, Y. Zhang, N. Wu, Y. Tao, and T. T. Truscott, "The upside-down water collection system of Syntrichia caninervis," *Nat. Plants*, vol. 2, no. 7, pp. 1–5, June 2016, doi: 10.1038/nplants.2016.76.

[17] C. Xu, R. Feng, F. Song, X.-L. Wang, and Y.-Z. Wang, "Desert Beetle-Inspired Superhydrophilic/Superhydrophobic Patterned Cellulose Film with Efficient Water Collection and Antibacterial Performance," *ACS Sustain. Chem. Eng.*, vol. 6, no. 11, pp. 14679–14684, Nov. 2018, doi: 10.1021/acssuschemeng.8b03247.
[18] A. W. Adamson, *Physical chemistry of surfaces*, 6th ed. New York: Wiley, 1997.
[19] C. S. Sharma, J. Combe, M. Giger, T. Emmerich, and D. Poulikakos, "Growth Rates and Spontaneous Navigation of Condensate Droplets Through Randomly Structured Textures," *ACS NANO*, vol. 11, no. 2, pp. 1673–1682, Feb. 2017, doi: 10.1021/acsnano.6b07471.
[20] *Advances in Contact Angle, Wettability and Adhesion*, 1st ed. John Wiley & Sons, Ltd, 2018. doi: 10.1002/9781119459996.
[21] S. Wang, K. Liu, X. Yao, and L. Jiang, "Bioinspired Surfaces with Superwettability: New Insight on Theory, Design, and Applications," *Chem. Rev.*, vol. 115, no. 16, pp. 8230–8293, Aug. 2015, doi: 10.1021/cr400083y.
[22] P.-G. De Gennes, F. Brochard-Wyart, and D. Quéré, *Capillarity and Wetting Phenomena*. New York, NY: Springer New York, 2004. doi: 10.1007/978-0-387-21656-0.
[23] D. Quéré, "Wetting and Roughness," *Annu. Rev. Mater. Res.*, vol. 38, no. 1, pp. 71–99, Aug. 2008, doi: 10.1146/annurev.matsci.38.060407.132434.
[24] J. Sun and P. B. Weisensee, "Tailoring wettability to push the limits of condensation," *Curr. Opin. COLLOID INTERFACE Sci.*, vol. 67, p. 101739, Oct. 2023, doi: 10.1016/j.cocis.2023.101739.
[25] H. J. Cho, D. J. Preston, Y. Zhu, and E. N. Wang, "Nanoengineered materials for liquid–vapour phase-change heat transfer," *Nat. Rev. Mater.*, vol. 2, no. 2, Dec. 2016, doi: 10.1038/natrevmats.2016.92.
[26] N. Miljkovic *et al.*, "Jumping-Droplet-Enhanced Condensation on Scalable Superhydrophobic Nanostructured Surfaces," *Nano Lett.*, vol. 13, no. 1, pp. 179–187, Jan. 2013, doi: 10.1021/nl303835d.
[27] T. M. Thomas and P. S. Mahapatra, "Condensation of Humid Air on Superhydrophobic Surfaces: Effect of Nanocoatings on a Hierarchical Interface," *LANGMUIR*, vol. 37, no. 44, pp. 12767–12780, Nov. 2021, doi: 10.1021/acs.langmuir.1c01012.
[28] J. B. Boreyko and C.-H. Chen, "Self-Propelled Dropwise Condensate on Superhydrophobic Surfaces," *Phys. Rev. Lett.*, vol. 103, no. 18, p. 184501, Oct. 2009, doi: 10.1103/PhysRevLett.103.184501.
[29] C. S. Sharma, C. W. E. Lam, A. Milionis, H. Eghlidi, and D. Poulikakos, "Self-Sustained Cascading Coalescence in Surface Condensation," *ACS Appl. Mater. INTERFACES*, vol. 11, no. 30, pp. 27435–27442, July 2019, doi: 10.1021/acsami.9b07673.
[30] D. Seo, J. Lee, C. Lee, and Y. Nam, "The effects of surface wettability on the fog and dew moisture harvesting performance on tubular surfaces," *Sci. Rep.*, vol. 6, no. 1, p. 24276, Apr. 2016, doi: 10.1038/srep24276.
[31] Y. Hou, M. Yu, X. Chen, Z. Wang, and S. Yao, "Recurrent Filmwise and Dropwise Condensation on a Beetle Mimetic Surface," *ACS Nano*, vol. 9, no. 1, pp. 71–81, Jan. 2015, doi: 10.1021/nn505716b.
[32] D. Nioras, K. Ellinas, and E. Gogolides, "Atmospheric Water Harvesting on Micro-nanotextured Biphilic Surfaces," *ACS Appl. Nano Mater.*, vol. 5, no. 8, pp. 11334–11341, Aug. 2022, doi: 10.1021/acsanm.2c02439.
[33] J. Estephan *et al.*, "Controlled wettability of biphilic patterned surfaces for enhanced atmospheric water harvesting," *MICRO NANO Eng.*, vol. 23, p. 100255, June 2024, doi: 10.1016/j.mne.2024.100255.

[34] B. Mondal, M. Mac Giolla Eain, Q. Xu, V. M. Egan, J. Punch, and A. M. Lyons, "Design and Fabrication of a Hybrid Superhydrophobic–Hydrophilic Surface That Exhibits Stable Dropwise Condensation," *ACS Appl. Mater. Interfaces*, vol. 7, no. 42, pp. 23575–23588, Oct. 2015, doi: 10.1021/acsami.5b06759.

[35] K. Hou, X. Li, Q. Li, and X. Chen, "Tunable Wetting Patterns on Superhydrophilic/Superhydrophobic Hybrid Surfaces for Enhanced Dew-Harvesting Efficacy," *Adv. Mater. INTERFACES*, vol. 7, no. 2, p. 1901683, Jan. 2020, doi: 10.1002/admi.201901683.

[36] R. Wen, S. Xu, D. Zhao, Y.-C. Lee, X. Ma, and R. Yang, "Hierarchical Superhydrophobic Surfaces with Micropatterned Nanowire Arrays for High-Efficiency Jumping Droplet Condensation," *ACS Appl. Mater. Interfaces*, vol. 9, no. 51, pp. 44911–44921, Dec. 2017, doi: 10.1021/acsami.7b14960.

[37] S.-F. Zheng, U. Gross, and X.-D. Wang, "Dropwise condensation: From fundamentals of wetting, nucleation, and droplet mobility to performance improvement by advanced functional surfaces," *Adv. Colloid Interface Sci.*, vol. 295, p. 102503, Sept. 2021, doi: 10.1016/j.cis.2021.102503.

[38] A. Abbatecola *et al.*, "Understanding the Role of Superhydrophobicity on Heat Transfer Enhancement During Dropwise Condensation in Humid Air Flow," *Adv. Mater. Interfaces*, vol. n/a, no. n/a, p. 2500270, 2025, doi: 10.1002/admi.202500270.

[39] N. Miljkovic and E. N. Wang, "Condensation heat transfer on superhydrophobic surfaces," *MRS Bull.*, vol. 38, no. 5, pp. 397–406, May 2013, doi: 10.1557/mrs.2013.103.

[40] J. Feng, Y. Pang, Z. Qin, R. Ma, and S. Yao, "Why Condensate Drops Can Spontaneously Move Away on Some Superhydrophobic Surfaces but Not on Others," *ACS Appl. Mater. INTERFACES*, vol. 4, no. 12, pp. 6618–6625, Dec. 2012, doi: 10.1021/am301767k.

[41] Y.-T. Cheng and D. E. Rodak, "Is the lotus leaf superhydrophobic?," *Appl. Phys. Lett.*, vol. 86, no. 14, p. 144101, Mar. 2005, doi: 10.1063/1.1895487.

[42] C. Dorrer and J. Rühe, "Some thoughts on superhydrophobic wetting," *Soft Matter*, vol. 5, no. 1, pp. 51–61, Dec. 2008, doi: 10.1039/B811945G.

[43] Y. Liu and C.-H. Choi, "Condensation-induced wetting state and contact angle hysteresis on superhydrophobic lotus leaves," *Colloid Polym. Sci.*, vol. 291, no. 2, pp. 437–445, Feb. 2013, doi: 10.1007/s00396-012-2751-6.

[44] T. M. Thomas, P. S. Mahapatra, R. Ganguly, and M. K. Tiwari, "Atmospheric water vapor condensation on engineered interfaces: Busting the myths," *Langmuir*, vol. 39, no. 15, pp. 5396–5407, Apr. 2023, doi: 10.1021/acs.langmuir.3c00022.

[45] J. Huang, J. Zhang, and L. Wang, "Review of vapor condensation heat and mass transfer in the presence of non-condensable gas," *Appl. Therm. Eng.*, vol. 89, pp. 469–484, Oct. 2015, doi: 10.1016/j.applthermaleng.2015.06.040.

[46] P. Poredoš, N. Petelin, T. Žel, B. Vidrih, P. Gatarić, and A. Kitanovski, "Performance of the Condensation Process for Water Vapour in the Presence of a Non-Condensable Gas on Vertical Plates and Horizontal Tubes," *Energies*, vol. 14, no. 8, Art. no. 8, Jan. 2021, doi: 10.3390/en14082291.

[47] M. B. Noremylia, M. Z. Hassan, and Z. Ismail, "Recent advancement in isolation, processing, characterization and applications of emerging nanocellulose: A review," *Int. J. Biol. Macromol.*, vol. 206, pp. 954–976, May 2022, doi: 10.1016/j.ijbiomac.2022.03.064.

[48] N. Grishkewich, N. Mohammed, J. Tang, and K. C. Tam, "Recent advances in the application of cellulose nanocrystals," *Curr. Opin. Colloid Interface Sci.*, vol. 29, pp. 32–45, May 2017, doi: 10.1016/j.cocis.2017.01.005.

[49] J. Tang, J. Sisler, N. Grishkewich, and K. C. Tam, "Functionalization of cellulose nanocrystals for advanced applications," *J. Colloid Interface Sci.*, vol. 494, pp. 397–409, May 2017, doi: 10.1016/j.jcis.2017.01.077.
[50] H. Dai *et al.*, "Recent advances on cellulose nanocrystals for Pickering emulsions: Development and challenge," *Trends Food Sci. Technol.*, vol. 102, pp. 16–29, Aug. 2020, doi: 10.1016/j.tifs.2020.05.016.
[51] L. Ming *et al.*, "Evolution and critical roles of particle properties in Pickering emulsion: A review," *J. Mol. Liq.*, vol. 388, p. 122775, Oct. 2023, doi: 10.1016/j.molliq.2023.122775.

Appendix: Error Analysis of CNC-wax Pickering Emulsion Particle Size Measurement

Objective of error analysis

The objective of this error analysis is to quantify the uncertainty associated with particle size measurements. This analysis provides context for the variability observed in the reported particle size distributions and supports reliable comparison between different emulsion formulation conditions. The error analysis is intended to assess measurement robustness and data consistency rather than to establish absolute particle size accuracy.

Sources of uncertainty

The primary source of uncertainty in the measured particle size distributions arises from procedural variability during emulsion preparation rather than from instrumentation or statistical analysis. Although identical formulation parameters were used, samples synthesized on different days exhibited noticeable differences in particle size distributions (Figure Aa), indicating sensitivity to small variations in experimental conditions during preparation.

Potential contributors to this procedural variability include minor fluctuations in mixing conditions, temperature, emulsification time, and dispersion efficiency, which can influence droplet breakup and stabilization during Pickering emulsion formation. These factors are difficult to control identically across separate synthesis batches and can lead to batch-to-batch differences in particle size.

In contrast, instrument-related uncertainty was found to be much less (Figure Ab). Repeated measurements of the same sample using identical imaging and image analysis procedures produced similar particle size distributions, suggesting that image resolution, calibration, and particle detection contribute negligibly to the overall uncertainty. As a result, the observed variability in particle size is attributed predominantly to sample-to-sample differences introduced during fabrication rather than measurement repeatability.

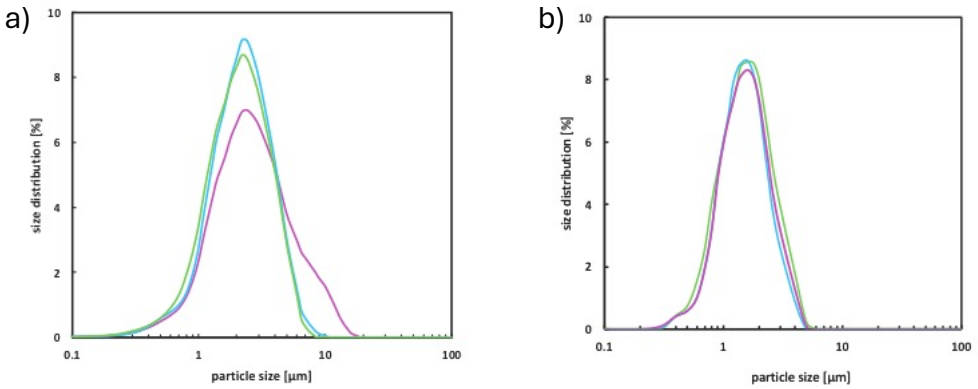


Figure A. Particle size distribution. Emulsion formula: 0.5% CNC, 47 mM NaCl, 15% oil fraction. a) single measurement of multiple emulsion samples; b) multiple measurements of one emulsion sample

Quantification of particle size distribution width

To quantitatively describe differences in particle size distributions among formulations, characteristic percentile diameters d10, d50, and d90 were extracted from each measured distribution. The d10 and d90 values represent the lower and upper bounds of the particle size population, while d50 corresponds to the median particle diameter. Together, these parameters provide a concise numerical description of both the central tendency and the spread of the distribution.

The width of each particle size distribution was evaluated using the difference between d90 and d10, which serves as a measure of distribution broadness. Formulations exhibiting a narrow, sharply peaked distribution show smaller d90–d10 values, whereas broader distributions are characterized by larger d90–d10 values. This metric enables direct comparison of distribution shape between different formulation conditions without assuming a specific distribution form.

For each formulation, the reported d10, d50, d90, and d90–d10 values correspond to the measured particle size distribution under the same analysis conditions. These numerical descriptors support qualitative observations from the distribution plots, such as peak sharpness and tail broadening, and provide a consistent basis for comparing the effects of formulation parameters on particle size uniformity.

Table A. Characteristic particle size metrics extracted from particle size distributions

Formulation	**D_{10} (µm)**	**D_{50} (µm)**	**D_{90} (µm)**	**D_{90}-D_{10} (µm)**
0.2% CNC, 47 mM NaCl, 10% oil fraction	1.14	2.77	4.84	3.70

0.35% CNC, 47 mM NaCl, 10% oil fraction	1.23	2.59	4.71	3.47
0.5% CNC, 47 mM NaCl, 10% oil fraction	1.20	2.45	5.24	4.04
0.7% CNC, 47 mM NaCl, 10% oil fraction	0.98	2.15	4.84	3.86
1% CNC, 47 mM NaCl, 10% oil fraction	0.91	1.99	4.48	3.57
1.3% CNC, 47 mM NaCl, 10% oil fraction	1.00	2.12	6.70	5.69
1.5% CNC, 47 mM NaCl, 10% oil fraction	0.89	2.05	6.87	5.98
1.7% CNC, 47 mM NaCl, 10% oil fraction	0.85	1.80	3.45	2.60
2% CNC, 47 mM NaCl, 10% oil fraction	0.88	1.89	3.72	2.84
ODA/oil = 0.005, ODA/CNC=0.05, 10% oil fraction	0.84	1.58	2.73	1.89
ODA/oil = 0.01, ODA/CNC=0.05, 10% oil fraction	0.71	1.42	2.57	1.87
ODA/oil = 0.005, ODA/CNC=0.08, 10% oil fraction	0.83	1.56	2.69	1.86
ODA/oil = 0.01, ODA/CNC=0.08, 10% oil fraction	0.76	1.43	2.48	1.73
ODA/oil = 0.005, ODA/CNC=0.1, 10% oil fraction	0.69	1.43	2.61	1.92
ODA/oil = 0.01, ODA/CNC=0.1, 10% oil fraction	0.65	1.29	2.32	1.66
ODA/oil = 0.03, ODA/CNC=0.1, 10% oil fraction	0.62	1.31	2.44	1.82
ODA/oil = 0.005, ODA/CNC=0.25, 10% oil fraction	1.37	2.16	3.34	1.97
ODA/oil = 0.01, ODA/CNC=0.25, 10% oil fraction	0.85	1.68	2.98	2.13
ODA/oil = 0.03, ODA/CNC=0.25, 10% oil fraction	0.65	1.63	4.01	3.36
ODA/oil = 0.005, ODA/CNC=0.5, 10% oil fraction	1.63	5.93	11.53	9.89
ODA/oil = 0.01, ODA/CNC=0.5, 10% oil fraction	1.45	2.67	4.83	3.38
ODA/oil = 0.03, ODA/CNC=0.5, 10% oil fraction	0.97	2.80	6.24	5.26